सत्यमेव जयते

ब्रिट बुलेटिन-2023

BRIT *Bulletin* 2023

वैज्ञानिक पत्रिका

Scientific Magazine

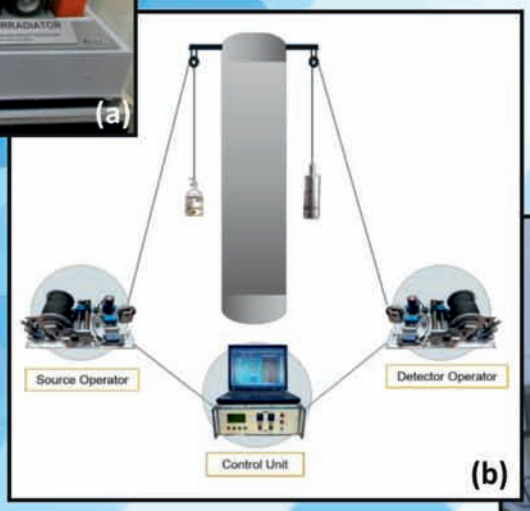

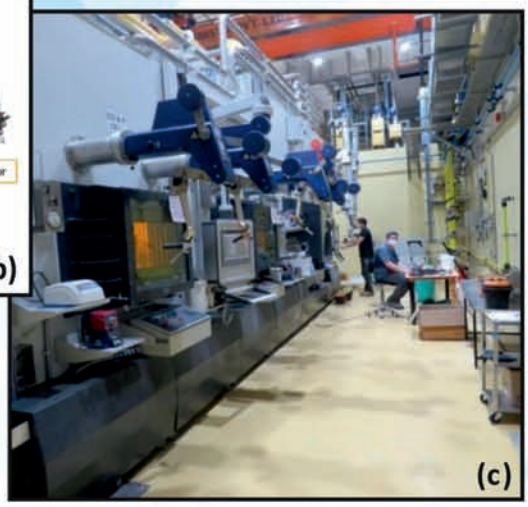

GOVERNMENT OF INDIA
DEPARTMENT OF ATOMIC ENERGY
BOARD OF RADIATION & ISOTOPE TECHNOLOGY

सत्यमेव जयते

ब्रिट बुलेटिन-2023

BRIT *Bulletin*- 2023

वैज्ञानिक पत्रिका
'Scientific Magazine'

विकिरण एवं आइसोटोप प्रौद्योगिकी बोर्ड, डीएई
Board of Radiation & Isotope Technology, DAE

GOVERNMENT OF INDIA

Front Cover: (a) Schematic view of Mobile Food Irradiator
(b) Gamma Scanning using Radioisotopes;
(c) Fission Molybdenum Plant Facility

Back Cover: Logos of (a) G 20 Summit & (b) Azadi ka Amrit Mahotsav

Foreword

It gives me pleasure and pride to release the Publication of BRIT Bulletin-2023, which houses, brief communications, original research articles, review articles and general/feature articles.

At BRIT, we have a variety of projects and initiatives in all the fields and these may be focused on product innovation & development. There is always an exciting opportunity for us to create something great together.

BRIT products exploit range of radioisotopes and devices which uses radiation technology for our esteemed customers for their varied applications. They are produced by skilled expertise and with stringent quality checks, to yield good quality products, which are comparable to any international products. This is the reason BRIT has wide array of customers, not only in India, but abroad, as well. The services are dedicated to societal benefits.

We need to use our creativity and problem-solving skills to develop new products and creativities that can help us succeed, while fulfilling the mandate of BRIT. Let's continue innovating, and please allow me to express my happiness to witness few of these being showcased in this Bulletin.

As we look ahead, it is important to stay diligent and committed to our objectives. Let's keep working together towards success!

I am happy to present you all 'BRIT Bulletin-2023', the contents of which continues to give an account of various R&D activities carried out at BRIT, along with General/Feature article, and important contributions from diverse areas of science.

I extend my appreciation to the Scientists and Engineers for their valuable contributions for BRIT Bulletin 2023.

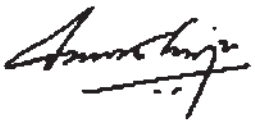

Pradip Mukherjee

CONTENTS

Brief Communication

1. Development of an Automated Potentiometric Method-based "Dose Measurement System" for Radiation Processing Plant **1-6**

   Ronie A. Ghosh, Rahul Kumar, P.K. Jothish

2. Synthesis of [^{14}C]-Fosthiazate **7-10**

   D. B. Kalgutkar, S. P. Patil, K. M. Mathew, N. Jayachandran

Original Research Article

1. Production of Pharmaceutical Grade [^{201}Tl]Thallous Chloride using 30 MeV Cyclotron **11-25**

   Sankha Chattopadhyay, Luna Barua, D.G. Mahesh, Shayantani Ash, Arpit Mitra, Sujata Saha Das, Samarjit Singha, Md. Neyar Alam, Madhusmita, Suprakash Roy, Prosenjit Dhang, Mukesh Jain

2. Temperature Profile of MTP-1200 Package for Normal Conditions of Transport **26-29**

   Prashant Dewan, Mukhar Sharma, Dhiren Sahoo

3. Development of ^{68}Ga-based Lyophilized Kit Formulation Towards PET Imaging of Tumor-Induced Angiogenesis **30-40**

   Soumen Das, Avik Chakraborty, Rubel Chakravarty, Sudipta Chakraborty

General Article

1. Air Conditioning and Ventilation Application for the Production of Radiopharmaceuticals **41-46**

   Babloo Kumar, Chetan Kothalkar, Aaditya Shah

Development of an Automated Potentiometric Method-based "Dose Measurement System" for Radiation Processing Plant

*Ronie A. Ghosh, Rahul Kumar, *P.K. Jothish*

Control & Instrumentation Group (C&I), ESSA; *Dosimetry Group, LC&TS

email: ronieaghosh@britatom.gov.in

Introduction

Board of Radiation and Isotope Technology (BRIT) is an industrial unit of Department of Atomic Energy (DAE), Government of India. Radiopharmaceuticals, labelled compounds and nucleotides, gamma chambers, blood irradiators, and radiography exposure devices are the major products that BRIT offers as part of its extensive product line. In addition to production of these goods, BRIT provides isotope application services, project consultancy services, radioanalytical services, calibration & dosimetry services, and radiation processing services to the various private sector industries. One of these services is to help in designing and to facilitate the construction of Radiation Processing plants (RPPs) in private sector. The first commercial-scale Gamma Irradiator (GI) for food processing, RPP is established in India at Vashi, Navi Mumbai. The facility was commissioned on January 1st, 2000, with the mandate of showcasing commercial viability of GI for food processing [1]. The organization offers radiation processing solutions to over 300 clients nationwide, catering to the irradiation needs of various products such as spices, ayurvedic raw materials, pet and animal feed, and packaging materials [2].

Food irradiation covers a wide range of applications in the dose range of 0.05-10 kGy, depending on the commodity and the objective of the treatment using radiation processing plant (RPP). The accurate and precise dose measurement is very important for measuring the absorbed dose in Gamma radiation processing facilities and plants. In India, Ceric-Cerous Sulphate dosimetry systems are provided by BRIT. Dosimeters are employed in the context of routine dosimetry, dose-mapping, and plant validation of industrial Gamma irradiators. The assessment of the absorbed dose in radiation-processed products utilizing dosimeters is a crucial aspect of the quality assurance and testing programme for industrial Gamma irradiators. The Ceric-Cerous dosimeters are formulated in accordance with the ISO/ASTM 51205:2009(E) standards [3], which are suitable for implementation over a broad range of radiation doses spanning from 1 to 45 kGy. The dosimeters possess traceability to the National Standard Laboratory, BARC, and provide a simplified and direct read-out mechanism. The Ceric-Cerous based dosimetry system comprises an electrochemical cell, as depicted in Fig. 1. The electrochemical cell is comprising of glass syringe, potential leads, dosimetry ampoule, irradiated and un-irradiated solution. The gamma irradiation reduces Ceric Sulphate solution to Cerous Sulphate, which is presented below

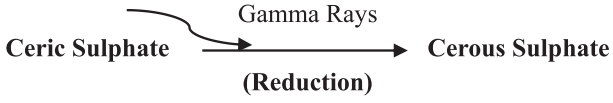

Methodology

Presently, BRIT uses and supplies Ceric-Cerous-based dose measurement system using the electrochemical cell and a millivolt meter. The present developed system utilizes the potentiometric method to measure the total radiation dose by determining the difference in electrochemical potential between an un-irradiated solution containing known concentrations of Ceric and Cerous ions, in comparison to gamma-irradiated solution, that initially contains the same known concentrations of Ceric and Cerous ions. The equipment consists of a compartmentalized cell that is partitioned into two distinct regions, which are demarcated by a permeable frit. The millivolt meter measures potential (in mV) between irradiated solution and un-irradiated solution. Millivolt to dose value is calculated using the equation (1) and this calculated dose reading is recorded in the register.

The dose measurement process followed at BRIT is quite time consuming and manual process, where, sometimes chances of human error increases due to human vision involvement. Commercially available Ceric-Cerous based dose measurement system consists of low precision voltmeter and its resolution is 0.1 mV. There is no possibility of upgradation of the method, which is available in the market. The Ceric-Cerous electrochemical cell is a very feeble voltage and current source, and that may need very high precision voltage measuring instrument so as to be able to measure the potential difference without loading the cell, and, therefore were getting erroneous measurement. Like any chemical cell it also tends to discharge when electric load is applied at the cell terminals.

Therefore, in order to overcome these problems, we have developed an improved milli-voltmeter with an extremely high input resistance input amplifier, precision analog to digital converter circuit, an embedded system, an isolated communication port and an in-house developed software-based readout and dose measurement system.

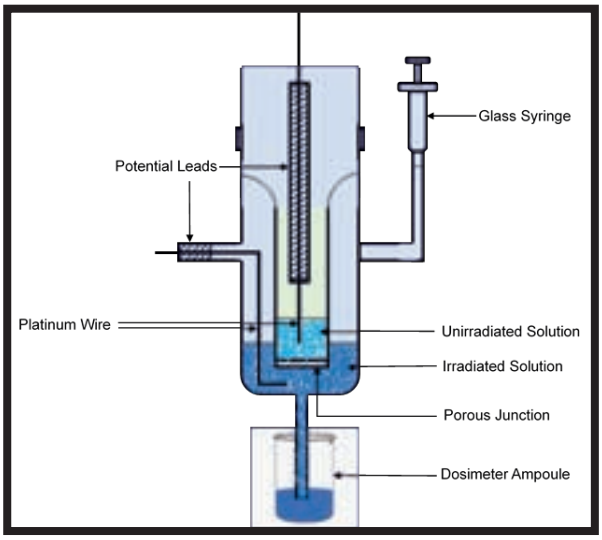

Fig. 1: Ceric-Cerous Electrochemical cell[3]

The comprehensive block diagram of the developed improved millivolt meter is shown in Fig. 2. The developed system having high-precision electronic digital milli-voltmeter and with resolution of 0.01 mV. Fig. 3. depicts the pictorial view of the in-house developed improved milli-voltmeter. In order to measure the total dose, the electric potential in the millivolt range generated by the solution separated by the porous frit can be accurately measured using a precision millivolt meter. As shown in Fig. 1., the electrical potential is generated within the designated potential leads. The measurement of this potential is conducted utilizing a high-precision digital millivolt meter with a range of 0-100mV, within an accuracy of 1%. The electrochemical cell has two compartments

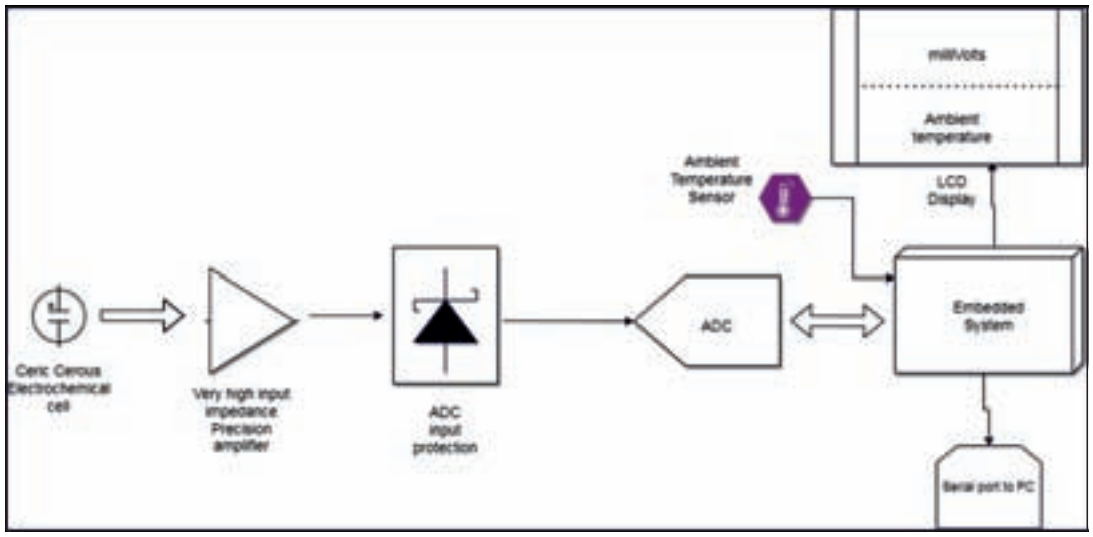

Fig. 2: Block diagram of the designed system

which are separated by a porous junction, such as a glass frit, a ceramic or kaolin junction, or a fiberglass wick. The inside section is always full of solution that has not been exposed to radiation. The solution to be tested is moved from an ampoule that has been irradiated or has not been irradiated into the lower section. A digital voltmeter is used to measure the electro potential that is made between the platinum electrodes in the two sections as shown in Fig. 1.

Both the compartments of electrochemical cells are filled with a dosimeter solution that has not been irradiated. To establish equilibrium across the porous junction, the solution is permitted to remain in the electrochemical cell for approximately 30 minutes. For the new batch of dosimeters or if a cell has not been used for at least a day, the solution should be left in both compartments for a minimum of 16 hours to ensure equilibrium across the porous junction. When the cell is being used for the first time, the filled cell must remain for at least 24 hours before measurements are taken. If the cell will not be utilized for longer than three days, the solution must be exhausted. Before reprocessing the cell, the inner and outer compartments must be rinsed three times with purified water and allowed to air dry. Failure to follow the procedures will result in inaccurate millivolt meter readings.

Design and Developmental Aspects

The developed electronic circuit containing a very high input impedance precision operational amplifier (OP-AMP), with extremely low offset and temperature drift has been incorporated at the input stage. It is followed by a Schottky diode-based protection clamp for Analog to Digital (ADC) converter input protection. The ADC converter converts the input analog voltage and amplified it by the input amplifier to binary digital form which is read by a microcontroller-based embedded system and is processed accordingly for a digital read out on the large graphics liquid crystal display (LCD). The temperature is also an important parameter, which may affect the dose measurement. Therefore, to compensate the temperature effect in the dose measurement, temperature sensor is also interfaced with the developed system and its digital readout on the same display

has been provided in accordance with point 10.5.8 of ASTM/ISO 51205-2017[3] for readout of temperature in the near vicinity of the electrochemical cell and then to apply correction for this temperature while recording the measurement. The temperature is measured using an extended temperature sensor probe attached near the electrochemical cell mount on the experiment table. Set up of the developed dosimetry system is shown in the Fig. 4.

When Ceric-Cerous Sulphate dosimeters are exposed to gamma radiation, Ceric ions are reduced to Cerous ions. The electrochemical potential difference *(ΔE)* between an unirradiated dosimeter solution and an irradiated solution, is used in the equation (1) to calculate the absorbed dose in kGy.

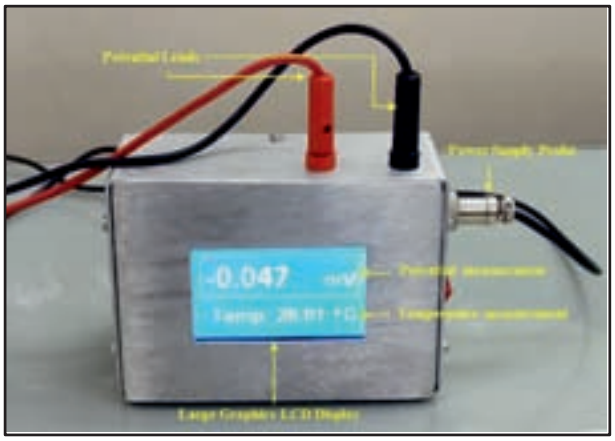

Fig. 3: Pictorial view of the indigenously developed improved millivolt meter device along with ambient temperature measurement for Ceric-Cerous based dosimetry system

Software Development

In BRIT, millivolt to dose measurement calculation has been done manually in accor-

$$Dose\ (kGy) = \frac{1}{\rho G[Ce^{+3}]}\left[[Ce^{+4}]_u - \left(\frac{[Ce^{+4}]_u + [Ce^{+3}]_u}{1+\frac{[Ce^{+3}]_u}{[Ce^{+4}]_u} antilog \frac{\Delta E}{59.16}}\right)\right] \quad \text{..... (1)}$$

where,

$\rho = Densityof\ the\ dosimetric\ solution\ (kg/m^3)$

$G[Ce^{+3}] = G\ value\ of\ Ce^{+3}\ (Radiochemical\ yield\ of\ the\ Cerous\ ion, mol/J$

ΔE = *Electrochemical potential difference (mV) at 25 °C*

$[Ce^{+4}]_u = Ceric\ \ ion\ concentration\ of\ unirradiated\ solution\ (mol/L)$

$[Ce^{+3}]_u = Cerous\ \ \ ion\ concentration\ of\ unirradiated\ solution\ (mol/L).$

Further, if ambient temperature is different (ideally it is 25°C), then to compensate the temperature effect on the dose measurement can be implemented by the equation (2).

$$\Delta E_{25°C} = \frac{\Delta E_t \times 298}{273+t} \quad \text{..... (2)}$$

where,

$\Delta E_{25°C}$ = mV reading at measuring temperature 25°C.

ΔE_t = mV readings at measuring temperature (t).

t = Measured ambient temperature.

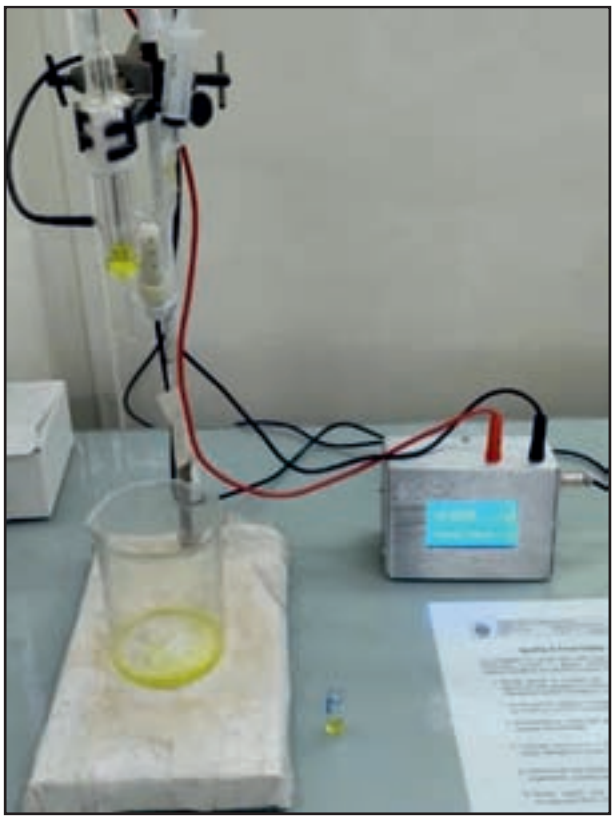

Fig. 4: Dose measurement setup of Ceric Cerous electrochemical cell and potentiometric measurement of dose using developed improve millivolt meter.

dance with the equation (1) and temperature correction is also calculated in accordance with equation (2) manually. Further, calculated dose is recorded in the register by the operator and there are always some possibilities of errors due to manual operations. So, for the ease of operation and minimize the human error in noting and calculation, we have developed a software, which provides an extensive solution to address this issue. The software is developed in the .NET framework 6.0 and used Visual Studio 2015. The program is written in the visual basic and computer configuration was windows 10 professional, 8 GB RAM, and 64-bit architecture. The developed millivolt meter is interfaced with the computer using RS-232 communication protocol.

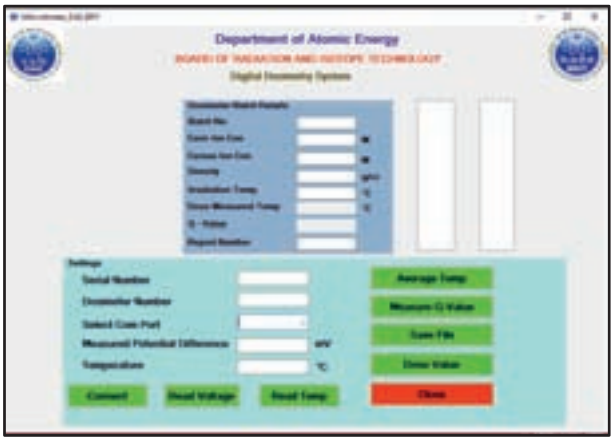

Fig. 5: Pictorial view of the indigenously developed improved millivolt meter device along with ambient temperature measurement for Ceric-Cerous based dosimetry system.

On the GUI initially user need to establish connection between millivolt meter and computer, so the user needs to select the COM port using the dropdown down box provided on the GUI. Afterwards click on the connect button and then enter all the relevant information e.g., batch number, Ceric ion concentration, Cerous ion concentration density, density, irradiation, temperature, temperature at the time of dose measurement, report number, serial number and dosimeter number. The G-value is calculating parameter, therefore we have disabled it so that the run time user cannot enter the value. Further, user can measure voltage and temperature reading for the relevant dosimetry readings are completed. Then click on the average temperature for doing averaging of the measurement temperature. Click on the "save file". A "save file" dialog will pop up and one may save the file on the desired location on the computer. After that click on the dose value correspondence dose value will be append in the saved text file. In this way, dose measurement may can be done using the developed improved millivolt meter and software. The graphical

user interface (GUI) of the developed software is shown in the Fig. 5.

Conclusion

- An improved milli-voltmeter based dosimetry system is successfully designed and developed.
- The developed system has a resolution of 0.01 mV.
- The temperature correction is also successfully implemented in the developed dosimetry system.
- Development of the software for the interfacing the developed millivolt meter and recording the measured dosimeter readings in the computer was found to be successful for n = 30 measurements.

References

1. https://www.barc.gov.in/pubaware/food.html Accessed on 20/02/2023.
2. https://www.britatom.gov.in/products Accessed on 20/06/2023.
3. ISO/ASTM. Standard Practice for Use of a Ceric-Cerous Sulfate Dosimetry System. 51205:2009(E): United States of America, 2009.

Synthesis of [^{14}C]-Fosthiazate

D. B. Kalgutkar, S. P. Patil, K. M. Mathew, N. Jayachandran

Labelled Compounds, LC & TS, BRIT

E-mail ID: dbkalgutkar@britatom.gov.in

Abstract

Fosthiazate labelled with Carbon–14, in its Thiazolidinone ring, was prepared using [^{14}C]-urea. A mixture of [^{14}C]-urea and cysteamine hydrochloride was cyclized to [^{14}C]-Thiazolidinone, which on treatment with sodium tert-butoxide, followed by O–ethyl S–sec butyl phosphorochloridothioate resulted in [^{14}C]-Fosthiazate. The product had specific activity of 5.64 μCi/mg and radiochemical purity greater than 99 %. The overall radiochemical yield was 43.3 %, based on [^{14}C]-urea.

Key words: [^{14}C]- urea, [^{14}C]- thiazolidinone, [^{14}C]- fosthiazate

Introduction

Annually, billions of livestock are destroyed by parasitic nematodes. Plant parasitic nematodes are even more destructive. The treatment for disinfestation of pests, either, prior to or at the stage of planting or transplanting of potatoes and tomatoes, was methyl bromide fumigation. Methyl bromide has been identified as a chemical that depletes earth's ozone layers. An alternative treatment is being searched. Also, due to the reduced availability and increased cost of use of Methyl bromide, its phase out process has started since 2005 for all uses.

Fosthiazate is a viable alternative to the use of methyl bromide for the control of nematodes infesting potato & tomato fields[1,2]. Fosthiazate is a new organophosphrous active ingredient that controls a broad spectrum of nematode species. It achieves the insecticidal effect by inhibiting synthesis of acetylchloneesterase in root-knot nematodes[3]. It is applied in the form of granules and aqueous emulsion. To study the amount of Fosthiazate remaining in soil due to chemical degradation, dissipation of the soil and to study chemical uptake into plants, [^{14}C]-Fosthiazate was required.

Fosthiazate labelled with Carbon–14, in its thiazolidinone ring was prepared [4] using [^{14}C]-urea. The reaction scheme is shown in Fig. 1.

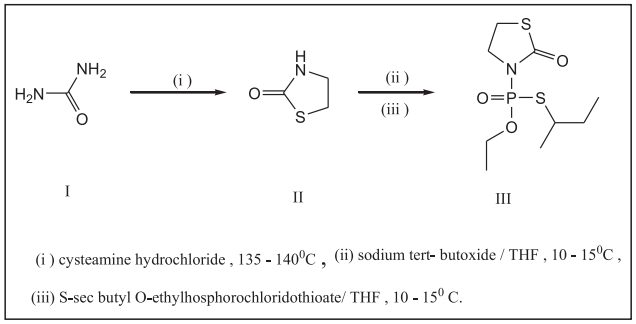

Fig. 1: Synthesis of [^{14}C]-Fosthiazate

A mixture [^{14}C]-urea and cysteamine hydrochloride was cyclized to [^{14}C]-thiazolidinone which on treatment with sodium tert-butoxide, followed by O–ethyl S–sec butyl phosphorochloridothioate, resulted in the production of [^{14}C] Fosthiazate.

Experimental

The radioactive starting material, [^{14}C]-urea, was prepared in-house by the

published reported procedure. Cysteamine hydrochloride, O–ethyl S–sec butyl phosphorochloridothioate and Fosthiazate and other chemicals were obtained from indigenous source. The radioactivity of [^{14}C]-Fosthiazate was measured with LSS 4029 liquid scintillation counter supplied by Electronics Division, BARC, INDIA. The radiolabelled compound was estimated using Shimadzu UV-VIS spectrophotometer (Model UV – 265). TLC analysis was performed on a silica gel 60F (Merck) plastic sheet. The radiochromatograms were scanned with a Bioscan radio chromatogram scanner (Model AR 2000). HPLC analysis was performed using a Dionex HPLC – system equipped with P680 HPLC pump and UVD 170U UV – detector. IR– spectra were recorded on infrared Schimadzu spectrophotometer. GC analysis was performed using Netel chromatographs instrument with DB-5 column, at injector temperature, 280^{0}C and column temperature 50^{0}C/min, -20^{0}C/min, -120^{0}C, -5^{0}C/min, –300^{0}C (10 min) (Model ULTRA – 2100).

[^{14}C]-Thiazolidinone

A mixture of vacuum-dried [^{14}C]-urea (3 mCi, 2 mmol, 120 mg) and dry cysteamine hydrochloride (242 mg, 2.14 mmol) was charged in a long-necked pyrex glass tube tapering at one end and having dimensions 15 cm OD and 20 cm long. It was heated at 135 – 140 ^{0}C for 18 hours in dry argon atmosphere. Dry argon atmosphere was continued while cooling. The solidified mass was stirred with dry acetone (15 ml) for 30 minutes and filtered to remove the solids. Solids were washed with dry acetone (2 X 15 ml) again. Acetone was removed in vacuo to get pale yellow titled product. It was then analyzed in silica gel TLC in the solvent system of dichloroethane: ethyl acetate (3:2), followed by autoradiography. It shows two spots – the major one of [^{14}C] thiazolidinone and minor one of [^{14}C]-urea. Radioactivity: 1.8 mCi. Radiochemical yield: 60 %. The product was used without purification for the next reaction.

[^{14}C]-Fosthiazate

To the cooled solution of [^{14}C]-thiazolidinone in dry tetrahydrofuran (2 ml) at 10^{0}C, sodium - tert butoxide (210 mg, 2.2 mmol) suspension in dry tetrahydrofuran was added and the reaction mixture was stirred for 1 hour at 10–15^{0}C. To this reaction mixture, O–ethyl S–sec butyl phosphorochloridothioate (450 mg, 2.4 mmol) was added and stirring was continued for two hours at the same temperature. Tetrahydrofuran was removed in vacuo. Water (15 ml) was then added and the product extracted with dichloroethane (3 X 15 ml). It was then analyzed by silica gel TLC in the solvent system of dichloroethane: ethyl acetate (3:2) followed by autoradiography. It showed two spots–the major one of [^{14}C]-fosthiazate and minor one of [^{14}C]- urea. The solvent was removed under reduced pressure and the product was loaded on to a silica gel column. Elution was performed with dichloroethane: ethyl acetate (3:2). The product was checked for radiochemical purity in the solvent system: dichloroethane: ethyl acetate (3:2) followed by radiochromatogram scanning. A single peak in the TLC radiochromatogram was obtained corresponding to the authentic sample. Radiochemical purity of the [^{14}C]-fosthiazate was estimated to be greater than 99%.

Results and Discussion

2-Thiazolidinone is useful as intermediate for medicine and agricultural pesticides such as fosthiazate[5]. It also has

good fungicidal activities towards various plant disease fungus. 2-Thiazolidinone [6,7] is synthesized by urea and cysteamine hydrochloride reaction with 60% yield. Since thiazolidinone is hygroscopic, it was vacuum-desiccated, prior to use and weighed and transferred in dry-box. Thiazolidinone formed a pale-yellow product, which was tried to distil out by vacuum distillation, but we were unsuccessful as solidification was observed in fractionating column. Hence, it was used without purification in the next step.

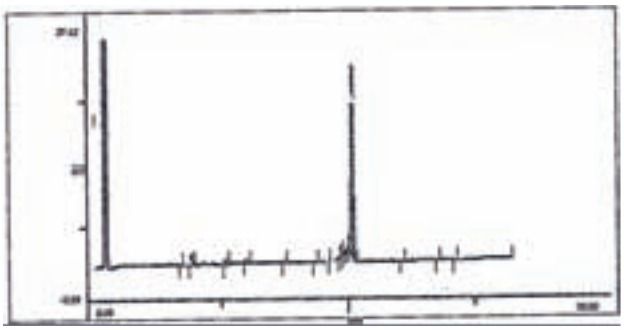

Fig. 2: Gas Chromatogram of Fosthiazate

In our cold synthesis, on two millimolar scale, the reaction product was identified as fosthiazate from its R_f value by comparison with the authentic sample. The pure product was obtained by preparative HPLC. Further confirmation was also obtained by melting point along with superimposable IR, UV and NMR spectra with an authentic sample. GC analysis was performed using DB-5 column, at injector temperature 280 ^{0}C and column temperature 50 ^{0}C (1 min) - 20 ^{0}C / min - 120 ^{0}C - 5 ^{0}C / min – 300 ^{0}C (10 min) and retention time of Fosthiazate was 15.28 min as shown in Fig. 2.

The radiolabelled compound was estimated spectrophotometrically at 222nm and radioactivity was measured by

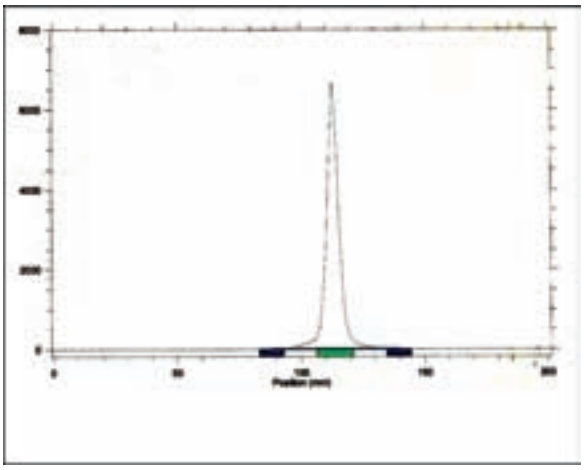

Fig. 3: Radio chromatogram of HPLC purified [^{14}C]-Fosthiazate

liquid scintillation counter. HPLC analysis was performed using C-18 reverse phase analytical column (25 cm X 0.46 cm) and acetonitrile (100%) as mobile phase at the flow rate of 1 ml / min and UV – detector set at 222nm. (retention time for fosthiazate = 3.8min). Radiochemical yield: 72.2%. Specific activity: 5.64 μCi / mg. Overall radiochemical yield of the [^{14}C]-fosthiazate was 43.3 %.

Acknowledgement

The authors wish to thank Shri. Pradip Mukherjee, Chief Executive, BRIT, for his kind support and encouragement.

References

1. Suijie Qin, Jianying Gan, W-ping Liu, Jiole Becker. **J. Agric. Food Chem. 52/20 (2004) 6239-6242.**
2. Christian Chabrier & Patrick Queneheve. **Nematropica 32/2 (2002).**
3. Woods A C, J R Frenels, M Ichinohe. **J. Nematology 23 (1991) 556.**
4. Kawamatsu Yutaka, Kogyo K K. **JP 58177983 (1983) 10-18.**
5. R Ottana, S Carotti, R Maccari, I Landini, G Chirocosta, B Caciagli, M G

Vigorita, E Mini. **Bio oran. Med. Chem. Lett. 15 (2005) 3930.**

6. M Yogisawa, M Kitano, T Morinoto, **EP 0387028 (1990) 9-12**.
7. J G Michels & G Gever, **J. Chem. Soc. 78 (1956) 5349.**

Production of Pharmaceutical Grade [^{201}Tl]Thallous Chloride using 30 MeV Cyclotron

Sankha Chattopadhyay[1], Luna Barua[1], D.G. Mahesh[1], Shayantani Ash[1], Arpit Mitra[2], Sujata Saha Das[1], Samarjit Singha[1], Md. Neyar Alam[1], Madhusmita[1], Suprakash Roy[3], Prosenjit Dhang[3], Mukesh Jain[4]

[1]Medical Cyclotron Facility, Regional Centre, Board of Radiation and Isotope Technology, Kolkata
[2]Radiopharmaceutical Laboratory, Board of Radiation and Isotope Technology, Navi Mumbai
[3]Medical Cyclotron Facility, Variable Energy Cyclotron Centre, Kolkata
[4]Department of Nuclear Medicine, Rabindranath Tagore International Institute of Cardiac Sciences, Kolkata

Email: sankha@vecc.gov.in

Abstract

Multiple patient doses of [^{201}Tl]TlCl has been produced using electrodeposited enriched ^{203}Tl in 30MeV cyclotron (Cyclone-30) with 28 MeV proton energy at 50 µA beam current for 8h. Ion Exchange Column Chromatography (IECC) and liquid-liquid extraction has been employed for semi-automated radiochemical separation and purification of produced [^{201}Tl]TlCl. The produced [^{201}Tl]TlCl was used in coronary artery disease (CAD) patients.

Introduction

Abnormalities in coronary blood flow were evaluated by myocardial perfusion imaging (MPI). The physiological conditions of myocardial function and its viability were assessed mainly by three different Food and Drug Administration (FDA) approved MPI agents namely (i) [^{201}Tl]Thallous Chloride ([^{201}Tl]Cl, Mallinckrodt Pharmaceuticals), (ii) [^{99m}Tc]Tc-Sestamibi ([^{99m}Tc]Tc-MIBI, Jubilant DraxImage Inc) and (iii) [^{99m}Tc]Tc-Tetrofosmin (GE Healthcare)[1,2]. Apart from these, various PET/CT MPI agents were developed and documented in pharmacopeias ([^{13}N]NH_3, [^{82}Rb]RbCl). However its use was restricted due to its limited availability owing to its very short half life[3].

[^{99m}Tc]Tc-MIBI is widely used due to widespread availability of sestamibi cold kits as well as [^{99m}Tc]TcO_4^- and is having relatively better myocardial extraction coefficient (MEC) of 65%. On the contrary, [^{201}Tl]TlCl has maximum MEC of 85%. Out of all these three MPI agents, but its clinical use was limited due to non-availability of indigenous source[4,5]. Nevertheless the promising *in-vivo* pharmacokinetic behavior of [^{201}Tl]TlCl has significant advantages over [^{99m}Tc]Tc-MIBI and [^{99m}Tc]Tc-Tetrofosmin, especially rapid clearance (92%) of [^{201}Tl]TlCl from blood within 5 minutes[2]. Moreover, [^{201}Tl]TlCl has an unique redistribution capability after several hours of intravenous administration as thallium-201 does not get trapped in myocytes and other tissues and this redistribution allows myocardial extraction in ischemic regions.

Hence, this property of Tl(I) allows [^{201}Tl]TlCl for acquiring redistribution SPECT/CT images for assessing tissue viability[6], as a result separate intravenous administration were not required for rest and stress SPECT/CT imaging[2].

The widespread use of [^{201}Tl]TlCl for regional blood flow, myocardial viability, and redistribution images (markers for regional viability) would have been possible with the development of stationary semiconductor technology based dedicated cardiac imaging system with cadmium-zinc-telluride[7]. The only limitations of [^{201}Tl]TlCl MPI agents was suboptimal SPECT/CT image quality due to low abundance (12%) of gamma photons of [^{201}Tl]TlCl (E_γ = 135 keV and 167 keV) compare to [^{99m}Tc]Tc-MIBI (E_γ = 140.5 keV, abundance = 89.1%)[6]. However, this limitation also could be overcome on using CZT cardiac scanner camera (D-SPECT) on injecting 0.9 – 1.0 mCi of [^{201}Tl]TlCl[8,9]. Even though [^{201}Tl]TlCl has relatively long physical half-life ($T_{1/2}$ = 73.06h) as compared to [^{99m}Tc]Tc-MIBI ($T_{1/2}$ = 6.04h), but whole body radiation dose was only 1.36 times higher for [^{201}Tl]TlCl (0.68 rad, on injecting single patient dose of 0.12 GBq) in comparison with [^{99m}Tc]Tc-MIBI (0.50 rad, on injecting single patient dose of 0.37 GBq)[2].

The availability of [^{99m}Tc]TcO_4^- for formulation of [^{99m}Tc]Tc-MIBI and [^{99m}Tc]Tc-Tetrofosmin was a challenging issues especially during the crisis of high specific activity (HSA) [^{99}Mo]MoO_4^{2-}, which is parent radionuclide for [^{99m}Tc]TcO_4^-. The sustainable production and availability of HSA [^{99}Mo]MoO_4^{2-} depend on availability of high enriched uranium (HEU) or low enriched uranium (LEU)[10]. The international safeguards on the use of HEU, has heavily impacted on the crisis and short supply of [^{99}Mo]MoO_4^{2-} worldwide[11]. To circumvent such crisis of [^{99}Mo]MoO_4^{2-}, many alternative radioisotopes namely Gallium-68, Copper-64, Iodine-123, Thallium-201, Flourine-18 etc., has gained prominence in application. Especially during the crisis of HSA [^{99}Mo]MoO_4^{2-}, [^{201}Tl]TlCl has played a pivotal role in diagnostic cardiac imaging[12].

Till the year 2020, India had to depend on the import of [^{201}Tl]TlCl for diagnostic studies in patients. However, after Cyclone-30 became operational, [^{201}Tl]TlCl was indigenously available to various nuclear medicine centers across India[5].

The production of ^{201}Tl is mainly done via the route ^{203}Tl(p,3n)^{201}Pb$\rightarrow$^{201}Tl, utilizing the energy range Ep = 28$\rightarrow$20 MeV[13]. The irradiation of ^{203}Tl is done at a medium-sized cyclotron to produce ^{201}Tl. Many radiochemical procedures for preparation of good quality ^{201}Tl raw material are available in the literature[14,15]. Irradiated thallium targets can be dissolved in diluted nitric acid, sulphuric acid or concentrated hydrogen peroxide. In Chemistry-I, the precipitation methodology where the intermediate no-carrier-added ^{201}Pb radioisotope produced after irradiation of ^{203}Tl is usually separated from the bulk quantity of ^{203}Tl by precipitating $PbSO_4$ after addition of lead carrier, co-precipitating with $Fe(OH)_3$ or $SrSO_4$, anion, cation exchange chromatography and adsorption chromatography are frequently applied. In Chemistry-II, column chromatography for separation of monovalent ^{201}Tl after reduction (with SO_2) from the ^{201}Pb bulk (upon decay of lead into thallium, a mixture of monovalent and trivalent thallium is obtained), and solvent extraction of trivalent ^{201}Tl (oxidation with

$KBrO_3$ or O_3 gas are applied. Upon reduction (with SO_2 and $NaHSO_3$), back-extraction is performed followed by ^{201}Tl bulk conditioning (pH and isotonicity adjustment, and sterilization). The present work, thus, describes the consistent and reliable production of Gigabecquerel level, clinical grade [^{201}Tl]TlCl injection from electroplated enriched ^{203}Tl target by proton irradiation using 30 MeV cyclotron. A semi-automated separation and purification of [^{201}Tl]TlCl module has been used following Ion Exchange Column Chromatography (IECC) and liquid-liquid extraction techniques. The quality control parameters of the produced [^{201}Tl]TlCl has been thoroughly validated and compared to the pharmacopeia standard. The excellent cardiac uptake in patient has proven the clinical efficacy of the indigenously produced [^{201}Tl]TlCl.

Materials and Methods

The base material made up of copper (purity: 99.99%, area: 11.69 cm^2) has been procured from IBA, Belgium. The ^{203}Tl as $^{203}Tl_2O_3$ (Enrichment: ~97%) has been obtained from Isoflex, USA. Hydrochloric acid (30%) of ultrapure grade (purity: ≥99.99% trace metal basis), Nitric acid (70%) of ultrapure grade (purity: ≥99.99% trace metal basis), Sulphuric Acid (96%) suprapure grade (Purity: 100%), Sodium hydroxide pellet of ensured grade (purity: ≥ 99%), disodium ethylenediamine tetraacetic acid (EDTA) dihydrate (Purity: ≥ 99%), diisopropyl ether (DIPE) (purity: ≥99.99% trace metal basis), water of ultrapure grade (Trace SELECT), acetone of ultrapure grade (purity: ≥99.99% trace metal basis) and Dowex 50W-X8 resin column (100–200 mesh, H^+ form) have been purchased from Sigma-Aldrich, USA. The following materials like sterile, pyrogen free single use 0.22 µm PES (Polyethersulphone) membrane syringe filter from Merck-Millipore, Germany; sterile, pyrogen free micropipette tips (Volume: 1000 µL and 250 µL) from Thermo Fisher, Germany; evacuated glass vials: sterile and pyrogen free (10 ml, vacuum <10 mbar, USP Type-I tubular glass vials) prepared in-house; sterile, pyrogen free bromobutyl rubber closures (diameter: 20 mm, 25 KGy γ irradiated) from Universal Medicap, India; sodium chloride injection IP (Intraperitoneal) (0.9% w/v) from NIVY Remedies Pvt. Ltd., India; Sulphur dioxide gas (SO_2, 100 mBar), Nitrogen gas (N_2, 30 mBar and 0.3 Bar) and Oxygen (O_2, 100 mBar for production of ozone) from Praxair, India have been used.

The Cyclone-30, IBA at Medical Cyclotron Facility, VECC, Kolkata, India, has been used for the production of ^{201}Tl. Instruments like dose calibrator (NaI detector), Capintec, USA; HPGe detector (p-type, co-axial) coupled to 4k channel MCA system - calibrated prior to use (ORTEC, Germany); gas chromatography (Model: YL6500, YOUNGIN Chromass, South Korea); ICP-AES (Model: ICAP duo 6500, Thermo Scientific, Germany); radio-chromatogram TLC scanner, Detector: BGO(V) (Ray Test-GITA, Germany); laminar air flow benches with adequate lead shielding (Microfilt, India) and twin chamber BOD (Biological Oxygen Demand) incubator (temperature: 37°C and 25°C), (Pooja Labs, India) have been used.

Preparation of Target

The target was prepared by electrodepositing isotopically enriched (97%, Isoflex, USA) metallic ^{203}Tl on copper base material (fabricated in-house,

area of electro-deposition: 11.69 cm^2) following the VUB (Vrije Universiteit Brussel) method (Manual, VUB, Belgium, 2008)[16] (Fig.1). The plating bath was prepared by dissolving 12 g of $^{203}Tl_2O_3$ in an aqueous alkaline solution containing a complexing agent (EDTA), an anodic depolarizer (hydrazine hydrate) and a wetting agent (BRIJ-35). From this bath, four targets are prepared by constant current electrolysis (current efficiency > 99%) involving the application of a bipolar chopped saw-tooth voltage between a central grounded Pt anode wire and four cathodes, i.e. four copper carriers, mounted vertically in appropriate windows of the electrodeposition vessel. The current density was adjusted to 3.17 mA/cm^2 and the electroplating took place with 99% current efficiency and the plating time was set for 6h. Every 1h, 300 µL of non-ionic surfactant (0.3% Brij-35, Sigma-Aldrich) was added. Thickness and uniformity of ^{203}Tl deposited in each target were measured using digital Vernier Caliper. The thermal shock test was carried out to check the adhesion of ^{203}Tl layer with the Cu base material.

Fig. 1. Electroplated enriched Tl-203 target

Cyclotron Irradiation

The electroplated ^{203}Tl solid target was irradiated in 30 MeV IBA cyclotron with 28 MeV proton energy at 50 µA beam current for 8h. After irradiation, the solid target mounted on a target carrier system (rabbit) was transported to the receiving hot cell from the irradiation station via an automated pneumatic transfer system without any manual intervention.

Radiochemical Separation and Purification of $[^{201}Tl]TlCl$

The two different semi-automated radiochemistry module was used for the radiochemical separation and purification of (I) $[^{201}Pb]Pb^{2+}$ from irradiated ^{203}Tl and (ii) $[^{201}Tl]Tl^{+}$ from $[^{201}Pb]Pb^{2+}$. The whole chemical process is carried out inside lead shielded hot-cell and controlled from a remote computer placed outside the hot-cell. All the operations were carried out using the GUI (Graphical User Interface) program installed in the computer. The steps involved in the semi-automated system for separation of $[^{201}Pb]Pb^{2+}$ from enriched ^{203}Tl target and $[^{201}Tl]Tl^{+}$ from $[^{201}Pb]Pb^{2+}$ are described below.

(I) Separation of $[^{201}Pb]Pb^{2+}$ from irradiated ^{203}Tl target (Chemistry-I)

Step 1: The irradiated target was loaded on the dissolution unit and 25 mL 0.7N HNO_3 (containing 100 mg $Pb(NO_3)_2$) transferred to the heated dissolution unit by operating the peristaltic pump to dissolve the target.

Step 2: The ^{201}Pb was precipitated as $[^{201}Pb]PbSO_4$ by using 10 mL of 3.6N H_2SO_4 under vigorous heating and stirring.

Step 3: The solubility of precipitated $[^{201}Pb]PbSO_4$ was reduced by transferring the suspension to the filtration unit through a spiral cooler. The $[^{201}Pb]PbSO_4$ precipitate in the filtration unit was collected on a cellulose filter (HVLP, 0.45µm) and washed 3 times with H_2O.

Step 4: The precipitate of $[^{201}Pb]PbSO_4$ was dissolved in 10 mL of 0.1M Na_2EDTA (pH ~9.0). Any co-precipitated Cu^{2+} (from

copper base material) was also dissolved due to the formation of EDTA-complex. Further second dissolution of $[^{201}Pb]PbSO_4$ precipitate was carried out using 10 mL of 0.1M Na_2EDTA (pH ~5.4), such that the resultant $[^{201}Pb]PbEDTA$ solution was free from any precipitate.

Step 5: SO_2 gas was bubbled through the resultant $[^{201}Pb]PbEDTA$ solution for reducing $[^{203}Tl]Tl^{3+}$ (trivalent form) to $[^{203}Tl]Tl^{+}$ (monovalent form). Homogenization of the $[^{201}Pb]PbEDTA$ solution was carried by bubbling N_2. The pH of the $[^{201}Pb]PbEDTA$ solution was maintained at 5.4 by using 1N NaOH

Step 6: The $[^{201}Pb]PbEDTA$ solution was loaded on a preconditioned Dowex-50W-X8 resin column. $[^{203}Tl]Tl^{+}$ cation was strongly adsorbed in the resin column while anionic $[^{201}Pb]PbEDTA$ and Cu-EDTA complexes were eluted into the volume measuring unit and homogenized by bubbling N_2.

The anionic $[^{201}Pb]PbEDTA^{2-}$ complex was stored at room temperature for 32h, so as $[^{201}Pb]Pb^{2+}$ was decayed to either $[^{201}Tl]Tl^{3+}$ or $[^{201}Tl]Tl^{+}$.

(ii) Separation of $[^{201}Tl]Tl^{+}$ from $[^{201}Pb]Pb^{2-}$ (Chemistry-II)

Step 1: SO_2 gas was bubbled through the $[^{201}Pb]PbEDTA$ complex after 32h of decay for reducing $[^{201}Tl]Tl^{3+}$ (trivalent form) to $[^{201}Tl]Tl^{+}$ (monovalent form), while The pH was maintained at 5.4 by using 1N NaOH.

Step 2: After reducing the radiothallium to monovalent form ($[^{201}Tl]Tl^{+}$), the $[^{201}Pb]PbEDTA$ complex was loaded on a preconditioned Dowex-50W-X8 resin column. The uncomplexed $[^{201}Tl]Tl^{+}$ was adsorbed on the resin column while $[^{201}Pb]PbEDTA$ and Cu-EDTA complexes were eluted in the waste flask[17].

Step 3: Resin column was washed with 35 mL of water to remove interstitial EDTA.

Step 4: The trapped $[^{201}Tl]Tl^{+}$ was eluted from the resin column using 15 mL 6N HCl, following which it was transferred to the solvent extractor.

Step 5: $[^{201}Tl]Tl^{+}$ was oxidized to $[^{201}Tl]Tl^{3+}$ by bubbling ozone gas for 1 min through the 6N HCl eluate (15 mL) collected in solvent extractor-**I**.

Step 6: 15 mL DIPE (DIPE saturated with 7N HCl) was introduced into the solvent extractor-**I**. The aqueous (acidic) and organic layers were mixed by bubbling N_2. $[^{201}Tl]Tl^{3+}$ was readily extracted from HCl (aqueous) into DIPE (organic) and the mixture was allowed to settle for 1min.

Step 7: After settling of the aqueous and organic layers, the aqueous layer was transferred to solvent extractor-**II**. Again 15 mL DIPE (DIPE saturated with 7N HCl) was introduced into the solvent extractor-**II**. The aqueous (acidic) and organic layers were mixed again the mixture was allowed to settle for 1min. Here second $[^{201}Tl]Tl^{3+}$ extraction was performed.

Step 8: After settling of aqueous and organic layers, the aqueous solution was transferred to the waste flask however the organic layer containing the $[^{201}Tl]Tl^{3+}$ remains in the extractor –**II**. Control of flow of the acidic aqueous and organic solution were monitored by the conductivity detector (CT) in the module which detects the conductance of aqueous solution and facilitate the transfer of aqueous layers to the waste flask by operating the solenoid valve.

Step 9: 10 mL of 0.005 N HCl was introduced into the solvent extractor-**II** containing organic phase (DIPE). SO_2 gas was bubbled through the aqueous layer

(0.005N HCl) for reducing [^{201}Tl]Tl^{3+} (trivalent form) to [^{201}Tl]Tl^{+} (monovalent form).

Step 10: The organic layer (DIPE) was mixed with aqueous layer (0.005N HCl) by bubbling N_2. [^{201}Tl]TlCl was back extracted from DIPE to 0.005N HCl. After separation of aqueous and organic layer, the aqueous acidic solution containing [^{201}Tl]TlCl was transferred into the product collection flask while DIPE was transferred to waste flask.

Step 11: Traces of DIPE from aqueous acidic solution (0.005N HCl) containing [^{201}Tl]TlCl, was removed by heating the solution at 90°C for 5 minutes.

Step 12: The pH of [^{201}Tl]TlCl was originally ~2.0 (in 0.005N HCl), which was brought to ~6.0 by adding 1N NaOH. The isotonicity of [^{201}Tl]TlCl was adjusted by adding sterile pyrogen free 0.9% NaCl. The resultant isotonic [^{201}Tl]TlCl was filtered using 0.22 µm PES membrane syringe filter to obtain 20 ml of [^{201}Tl]TlCl radiopharmaceutical.

Physicochemical and Biological Quality Control of [^{201}Tl]TlCl

The RCP (Radiochemical Purity) was evaluated by paper chromatography (PC) using Whatmman-3 (Strip Size: 8 x 90 mm) and 10% Na_2HPO_4: Acetone (1/9, v/v) as mobile phase. RNP (Radionuclidic Purity) was ascertained by performing γ-spectroscopy using high purity germanium (HPGe) detector coupled to 4k multiple channel analyzer (MCA) at 300s and 54000s (ORTEC). γ- spectroscopy for decayed samples of [^{201}Tl]TlCl were also carried out to rule out any long lived radionuclide impurities. Metallic impurities (Fe, Cu, Pb and Tl) were determined by Inductively Coupled Atomic Emission Spectrometry (ICP-AES) (Thermo Fisher Scientific). Residual DIPE levels were detected by gas chromatography (Youngin Chromass) using a standardized procedure with nitrogen as carrier gas. Endotoxin limit (EL) was quantified by Gel-clot BET (Bacterial Endotoxin Test) assay (Charles River). Sterility test was performed by direct inoculation method (Himedia). *In-vitro* stability of the product (RCP) on storage at controlled temperature (2°C – 8°C) was evaluated by radio-PC at 7 days' post production. Apart from RCP, sterility of the final product was assured post 7 days of production.

Clinical Studies of [^{201}Tl]TlCl in Patients: Methodological Considerations

Multiple patient doses (~9.78 GBq) of [^{201}Tl]TlCl were formulated per batch, using commercial semi-automated radiochemistry module from VUB Belgium. From the preparation, diagnostic doses of [^{201}Tl]TlCl (~ 0.12 GBq per patient) were administered in patient, with known cases of CAD. The clinical SPECT/CT imaging studies of CAD patient injected with [^{201}Tl]TlCl were carried out using a dedicated GE Discovery 670DR SPECT/CT scanner.

Results and Discussion

Most of the reported literature describes the commercial production of Tl-201 via ^{203}Tl (p,3n) ^{201}Pb → ^{201}Tl nuclear reaction. However, apart from radiochemical purification methodology employing IECC and LLE techniques, various groups has reported different radiochemical separation and purification strategy namely microporous hollow fibres -based solvent extraction[18], sorption in ammonium 12-molybdophosphate (AMP)[19], electromigration techniques[20].

However in the last three decades different solvents namely butyl acetate [21], N-benzylaniline[22] was experimented for LLE process but none of them resulted in better extraction of [^{201}Tl]Tl^{+} from ^{201}Pb. Also non-conventional production route like ^{201}Hg (p,n) ^{201}Tl, ^{202}Hg (p,2n) ^{201}Tl, ^{200}Hg (d,n) ^{201}Tl and ^{201}Hg (d,n) ^{201}Tl[23,24] for producing no carrier added (nca) ^{201}Tl were explored and subsequent radiochemical separation using liquid anion exchanger (trioctylamine) were studied to obtain high separation factor but the presence of 0.3 ppm of stable Hg in the final product ([^{201}Tl]TlCl) was major hindrances for clinical use[24]. Nevertheless, IECC and LLE techniques has proven to be commercially viable and has been adapted for developing semi-automated or automated modules for radiochemical separation and purification of [^{201}Tl]TlCl. Currently commercial radiochemistry module (VUB, Belgium) for radiochemical separation and purification of [^{201}Tl]TlCl based on IECC and LLE techniques using cation exchanger (Dowex 50W-X8 resin,100–200 mesh, H^{+} form) and diisopropyl ether (DIPE), respectively, is available.

The present work describes the production and radiochemical separation of Pb-201 from enriched Tl-203 target using IECC techniques and further separation of Tl-201 from Pb-201 using IECC (Dowex 50W-X8 resin) and LLE (DIPE) techniques.

Targetry and Irradiation

The 901.03 ± 0.95 mg (n = 8) of enriched ^{203}Tl was uniformly electro-deposited in an area of 11.69 cm^2 on the copper. Uniformly 75.95 ± 0.24 μm (n = 8) thick enriched ^{203}Tl was electrodeposited on the copper target within 6h by applying 3.17 mA / cm^2 of current density with > 99% current efficiency. The deposition rate of enriched ^{203}Tl on the copper target was 4.055 ± 0.001 mg / mA.h (n = 8). Uniform current density of 3.17 mA / cm^2 were maintained on adding 0.3 mL of 0.3% non-ionic surfactant at every 1 h interval. Typical electrodeposited (enriched ^{203}Tl) target is shown in **Fig. 1** indicating uniform morphology with no sign of adhesion and bubbles. Neither crack nor peeling off was observed from the target, post irradiation. Irradiation with 50 µA beam current yielded up to 237.4 ± 0.58 GBq (n = 8) of ^{201}Pb (non-decay corrected) at the end of bombardment (EOB).

Automated Separation and Purification of [^{201}Tl]TlCl

The chemical processing for separation and purification of [^{201}Tl]TlCl includes two steps of chemistry : In Chemistry-I, fast separation of ^{201}Pb ($T_{1/2}$ = 9.4h) from the irradiated ^{203}Tl target material after the end of the bombardment, and in Chemistry-II, the separation of no-carrier-added ^{201}Tl from the remaining ^{201}Pb after an appropriate grow-in period (32 h, only about 90% of the ^{201}Pb has decayed into ^{201}Tl) and the product [^{201}Tl]TlCl is isolated. the Chemistry-I involves the dissolution of enriched irradiated ^{203}Tl in diluted nitric acid containing a suitable amount of Pb-carrier, followed by the precipitation of ^{201}Pb as $PbSO_4$. To remove co-precipitated ^{203}Tl, a chromatographic purification step is performed. The $PbSO_4$ is dissolved in EDTA and the Tl^{3+} is reduced to the monovalent state by SO_2 gas. After pH adjustment, the solution is applied to a cation exchanger column. Co-precipitated $^{203}Tl^{+}$ is strongly adsorbed on the ion exchanger while the anionic $PbEDTA^{2-}$

complex is collected into the eluate. The latter is stored for decay of ^{201}Pb into ^{201}Tl.

^{201}Pb was separated from ^{203}Tl using computer controlled, semi-automated radiochemistry module of VUB, Belgium (Chemistry-I). Post 32h of decay of ^{201}Pb to mixture of $^{201}Tl^{3+}$ and $^{201}Tl^{1+}$, another different semi-automated radiochemistry module of VUB, Belgium (Chemistry-II) was used to separate $[^{201}Tl]Tl^{1+}$ from Pb (lead) and $[^{201}Tl]Tl^{3+}$. Chemistry-II involves a chromatographic adsorption of the formed, and by SO_2 reduced, $^{201}Tl^{+}$ on a cation exchanger, followed by a solvent extraction of the oxidized $^{201}Tl+$ into $^{201}Tl^{3+}$ using the HCl/DIPE system. ^{201}Tl is back-extracted into 0.005N HCl after reduction of Tl to the monovalent state. Simple bubbling of nitrogen gas through the bulk solution of $[^{201}Tl]Tl(I)Cl$ would not remove traces of DIPE as instructed in VUB Tl-201 production manual that is why in the present work the heating of the bulk solution was attempted. After that bulk conditioning involves pH and isotonicity adjustment of the $[^{201}Tl]Tl(I)Cl$ bulk solution.

Table 1. Production and Quality Control data of $[^{201}Tl]TlCl$

Production Batch No	Activity (^{201}Pb) at EOB (GBq)	Activity (^{201}Tl) before purification (GBq)	Activity (^{201}Tl) at EOP (GBq)#	RCY* (%)	RCP (%)	RNP (%)
1	236.8	20.09	9.02	44.89	99.78	99.59
2	237.8	20.17	9.98	49.47	99.04	99.67
3	237.2	20.86	10.01	47.98	99.61	99.58
4	237	20.11	9.86	49.06	99.80	99.65
5	238.2	20.21	10.28	50.86	99.81	99.80
6	237.9	20.18	10.06	49.85	99.56	99.52
7	236.5	20.06	8.99	44.81	99.19	99.21
8	237.5	20.15	10.10	50.12	98.92	99.37
	Mean ± SD			**48.38 ± 2.57**	**99.33 ± 0.39**	**99.71 ± 0.18**

EOB: End of Bombardment, EOP: End of Purification, #: Activity at EOP in 20 mL, RCY*: Non-Decay corrected radiochemical yield

Quality Control Parameters of [^{201}Tl]TlCl		Specifications of [^{201}Tl]TlCl based on USP*/EP$/Intl. P#[25,26,27]		Production results of Pharmaceutical Grade [^{201}Tl]TlCl
Non-Decay Corrected RCY (%)		NA		4.11 ± 0.19%
Appearance		Clear and Colorless*$#		Clear and Colorless
pH		4..5 – 7.5*		5.0 - 6.5
RNI		70 – 75 hours$		73 – 74 hours
RNP		^{202}Tl	< 2.0%$#	99.71 ± 0.18%
		^{200}Tl & ^{203}Pb	< 1.0%$#	
RCP (radio-PC)		> 95%*$#		99.33 ± 0.39%
Specific Activity (GBq / μg)		≥ 0.004#		1.43 ± 0.26 GBq / μg
Residual Solvent Levels	DIPE	NA		5.61 ± 0.52 ppm
Metallic impurities (μg / mL)	Tl	< 2.0*#		0.35 ± 0.07 μg / mL
	Fe	< 5.0*#		0.59 ± 0.05 μg / mL
	Cu	< 5.0*#		0.04 ± 0.03 μg / mL
	Pb	NA		0.05 ± 0.02 μg / mL
Bacterial Endotoxin Level		< 175 EU/V*#		< 6 EU/mL
Sterility (Post-facto)		No growth observed in 14 days*#		Complies
In-vitro Stability	RCP shall be > 95%, 7d post production on storage at (2-8°C)	> 95%#		98.61 ± 0.46%
	RNP shall be > 97%, 7d post production on storage at (25°C)	> 97%#		98.85 ± 0.07%

The first stage of radiochemical and separation process (Chemistry-I) was based on ion exchange chromatography only, while Chemistry-II process was carried out using ion exchange chromatography and solvent extraction.

In Chemistry-I, IEEC was employed, while in Chemistry-II, both IEEC and LLE were carried out to remove wide variety of contaminants like ^{203}Tl, Pb & $[^{201}Tl]Tl^{3+}$ from the produced $[^{201}Tl]TlCl$. Such multistage separation and extraction process was essential to get the produced $[^{201}Tl]TlCl$ in purest form, so as the RNP and RCY of the produced $[^{201}Tl]TlCl$ were in accordance with pharmacopeias, USP, EP, IP[25,26,27]. The loss of Tl-201 in Chemistry-II has been found to be around 50%. Each of the chemistry processes was achieved within 50 ± 5 min (n = 8). At the end of purification (EOP) the produced pharmaceutical grade $[^{201}Tl]TlCl$ for all the produced batches were 9.78 ± 0.49 GBq, while the non-decay corrected radiochemical yield (RCY) were in the range of 48.38 ± 2.57% (n = 8) and were given in Table 1.

Quality Control of $[^{201}Tl]TlCl$

The pharmaceutical grade $[^{201}Tl]TlCl$ was found to be clear and colorless, while pH was maintained between 5.0 – 7.0. The radioactive concentration (RAC) for all the produced batches were in the range of 0.49 ± 0.02 GBq / mL.

Radiochemical Purity, Chemical Purity, *In-vitro* Stability and Residual Solvents Levels of $[^{201}Tl]TlCl$

The RCP of $[^{201}Tl]TlCl$ (n = 8), estimated by radio-PC was 99.33 ± 0.39% with R_f between 0.20 - 0.30 (Fig. 2A). In all the produced $[^{201}Tl]TlCl$ batches (n = 8), the levels of Fe, Pb, Cuand Tlwere 0.59 ± 0.05, 0.05 ± 0.02, 0.04 ± 0.03 and 0.35 ± 0.07 μg/mL of radioactive $[^{201}Tl]TlCl$ solution respectively. The observed Fe, Pb and Cu levels in radioactive $[^{201}Tl]TlCl$ batches were much below the specified limit of <5 μg/mL, while Tl content were also below the specified limit of <2 μg/mL (United State Pharmacopeia 29 National Formulary 24, 2006, pp. 2108; Pharmacopoeia, 2002; 4th International Pharmacopoeia, 2009, pp. 1-5) The radio-PC of $[^{201}Tl]TlCl$ was found to be 98.61 ± 0.46% (n = 8) and exhibited single peak with R_f : 0.26 (Fig. 2B) upto 7d post production upon storage at 2°C-8°C.

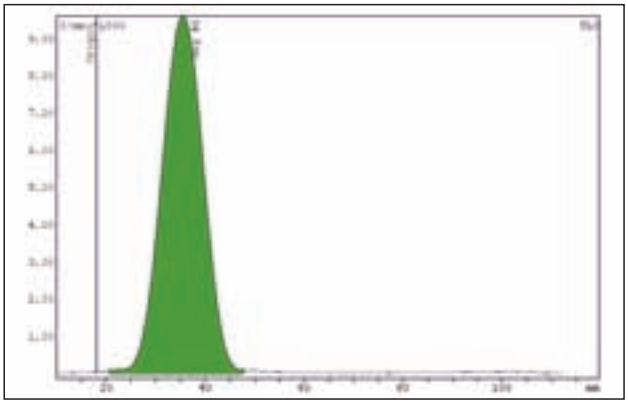

Fig. 2A. Radio-PC chromatogram of $[^{201}Tl]TlCl$ in 10% Na_2HPO_4: Acetone : 1/9 (v/v). R_f = 0.25

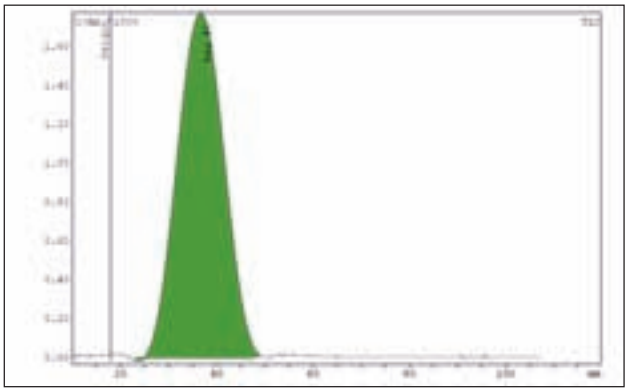

Fig. 2B. Radio-PC chromatogram of $[^{201}Tl]TlCl$ (R_f: 0.26) at 7d post production on storage at 2°C - 5°C

The measured half-life of [^{201}Tl]TlCl was between 73 – 74h. The EL of [^{201}Tl]TlCl was < 6 EU/mL. Residual DIPE levels in the [^{201}Tl]TlCl (n = 8) were 5.61 ± 0.52 ppm with R_t of 2.53 minutes (Fig. 2C) which was much below the permissible limits of 98 ppm.[25]. The specific activity of the produced [^{201}Tl]TlCl was 1.43 ± 0.26 GBq/μg which was well within the specified limit (> 0.004 GBq/μg) as described in pharmacopoeia[28].

The product was found to be sterile till 7d post production upon storage at controlled room temperature (2°C-8°C). The sterility of the product was not evaluated beyond 7d post production, hence sterility could not have claimed after 7d of production.

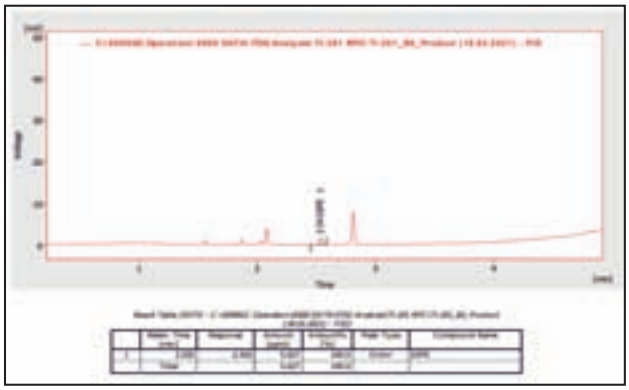

Fig. 2C. A typical gas chromatogram of [^{201}Tl]TlCl indicating residual DIPE levels (5.6 ppm)

Radionuclide Purity of [^{201}Tl]TlCl

The RNP of [^{201}Tl]TlCl (n = 8) derived by γ- spectroscopy was 99.54 ± 0.18% on counting for 300 seconds (Fig. 3A), while RNP for all the produced batches was 99.16 ± 0.21% on counting for 54000 seconds (n = 8) (Fig. 3B). Also the RNP (n = 8) of [^{201}Tl]TlCl was found to 98.85 ± 0.07% at 7d post-production (Fig. 3C). The possible radionuclide impurities could be present in our final purified [^{201}Tl]TlCl was ^{200}Tl ($t_{1/2}$: 1.09d), ^{202}Tl ($t_{1/2}$: 12.2d), ^{201}Pb ($t_{1/2}$: 9.4h) and ^{203}Pb ($t_{1/2}$: 2.17d) [29].

In our optimized irradiation and radiochemical separation method the percentage for the formation of ^{202}Tl, ^{200}Tl and ^{203}Pb were found to be < 0.12%, < 0.17% and < 0.20%, respectively in the final product by optimizing incident proton energy at 28 MeV on the target during irradiation for 8h and restricting the maximum proton energy to 24 MeV at the exit. Also decay time of 32h post Chemistry-I, contributed to maintain RNP of final [^{201}Tl]TlCl > 99%[30].

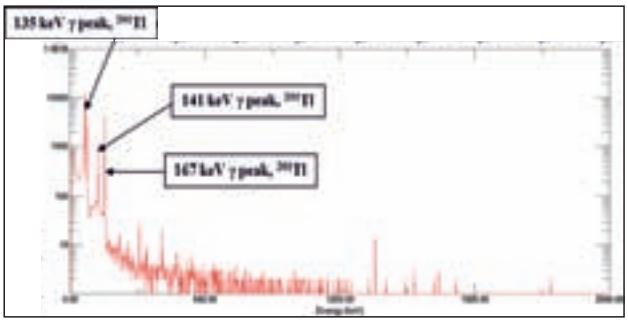

Fig. 3A. Gamma spectrum of [^{201}Tl]TlCl counted for 300s immediately after processing using 4k MCA

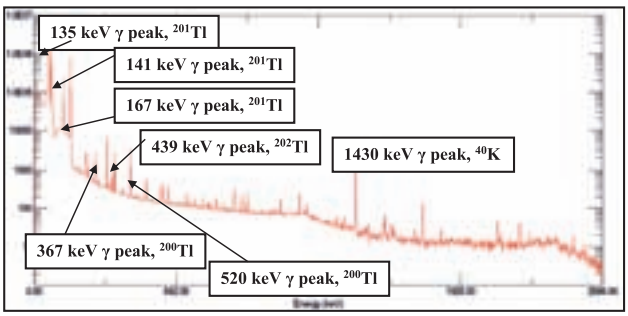

Fig. 3B. Gamma spectrum of [^{201}Tl]TlCl counted for 54,000s using 4k MCA

European Pharmacopeia describes, the permissible limit of ^{202}Tl was < 2% (Pharmacopoeia, 2002), whereas the United State Pharmacopeia defines the permissible limit of ^{202}Tl and ^{200}Tl were < 2.7% and < 2%, respectively (United State Pharmacopeia 29 National

Formulary 24, 2006, pp. 2108). Maintaining < 2% radionuclide impurities of ^{200}Tl (E_γ = 368 KeV) and ^{202}Tl (E_γ = 440 KeV) helped us to avoid contrast degradation in reconstructed [^{201}Tl]TlCl SPECT/CT images[31].

Table 2 demonstrates the quality control results of in-house produced [^{201}Tl]TlCl. The quality of the produced [^{201}Tl]TlCl was compared in Table 2 with the specifications as stated in the pharmacopoeias (United State Pharmacopeia 29 National Formulary 24, 2006, pp. 2108; Pharmacopoeia, 2002; 4th International Pharmacopoeia, 2009, pp. 1-5).

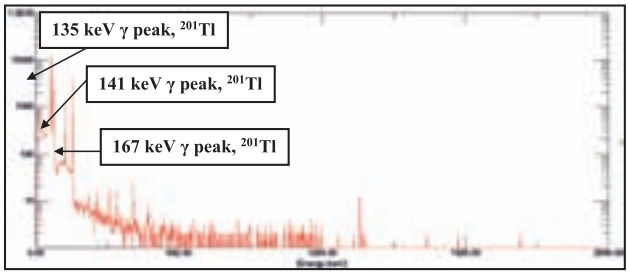

Fig. 3C. Typical gamma spectrum of [^{201}Tl]TlCl counted for 300s at 7d post processing using 4k MCA

[^{201}Tl]TlCl SPECT/CT Image of Patient

Clinical usage of [^{201}Tl]TlCl for MPI has seen growth in nuclear medicine centers having dedicated D-SPECT camera. However at nuclear medicine centers with SPECT/CT camera the usage of [^{201}Tl]TlCl for MPI is limited[8].

For our work, one clinical example was illustrated to prove the clinical outcome of the produced [^{201}Tl]TlCl. SPECT/CT imaging studies were carried out in an adult patient with suspected CAD. In same patient, [^{201}Tl]TlCl SPECT/CT imaging was carried out at "Rest" (Fig. 4A) and compared to that of [^{99m}Tc]Tc-MIBI SPECT/CT "Stress" (Fig. 4A) and "Rest" (Fig. 4B) scan . The produced [^{201}Tl]TlCl exhibited excellent uptake at "Rest" conditions and comparable to that of [^{99m}Tc]Tc-MIBI of the same patient at both the conditions. Also from the figures, it was observed that the uptake of [^{201}Tl]TlCl in liver and soft tissues of the same patient was low compared to [^{99m}Tc]Tc-MIBI at both the conditions (Rest and Stress).

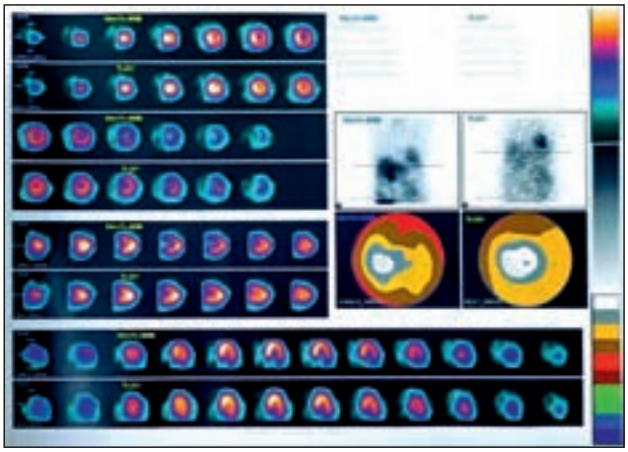

(A)

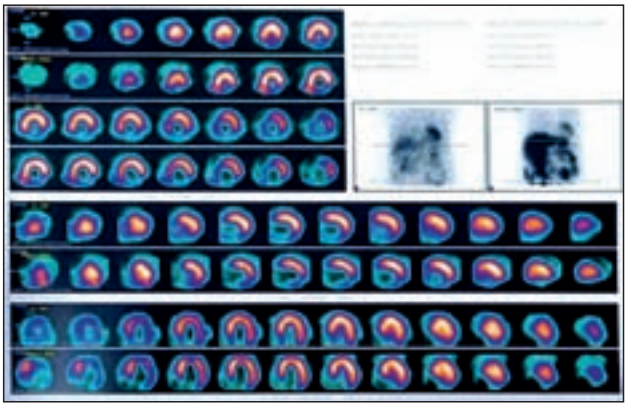

(B)

Fig. 4. CAD patient with excellent cardiac uptake of A. [^{201}Tl]TlCl at "Rest", while uptake at soft tissue and kidney were minimum compared to that of [^{99m}Tc]Tc-MIBI SPECT/CT scan B. "Rest" and A. "Stress" condition of same patient.

Conclusions

The semi-automated radiochemical separation and purification methodology employing IECC and LLE techniques has

been found to be suitable to produce high quality [^{201}Tl]TlCl. A reliable and efficient production route has been established and validated for producing multiple patient doses of pharmaceutical grade [^{201}Tl]TlCl. The current work thus demonstrates that the regular production and uninterrupted supply of patient doses of [^{201}Tl]TlCl could be possible using 30MeV Cyclotron for cardiac SPECT/CT imaging studies at nuclear medicine centers. Hence to conclude, the pharmaceutical grade [^{201}Tl]TlCl has been used for diagnosing a suspected CAD patient and can be useful for further future studies in this field.

Acknowledgements

The support and encouragement of Pradip Mukherjee, Chief Executive, Board of Radiation & Isotope Technology and Dr. Sumit Som, Director, Variable Energy Cyclotron Centre are being gratefully acknowledged. The authors thank Dr Susanta Lahiri, Former Professor, Saha Institute of Nuclear Physics, Kolkata for the support in conducting ICP-AES studies. The authors also thank the staff of the Production Group of Board of Radiation & Isotope Technology and Variable Energy Cyclotron Centre at Medical Cyclotron Facility, Chakgaria, Kolkata for support in carrying out the work.

References

1. Kostkiewicz, M. Myocardial perfusion imaging in coronary artery disease. **J Crvasa. 57 (2015) e446-e442.**
2. Baggish, A.L., Boucher, C.A. Radiopharmaceutical agents for myocardial perfusion imaging. **Circulation 118 (2008) 1668-1674.**
3. Mikolajczak. R., Garnuszek, P. Radiopharmaceuticals in cardiology. **Nucl. Med. Rev. 15 (2012) 39-45.**
4. Schwaiger M., Melin J. Cardiological applications of Nuclear Medicine. **Lancet 354 (1999) 661-666.**
5. Feedback of Thallium chloride (Tl-201).pdf https://britatom.gov.in/excellent-feedback-thallium-201-chloride-tl-201-radiopharmaceutical **(accessed 12 August 2023).**
6. Verberne, Hein J. et al. EANM procedural guidelines for radionuclide myocardial perfusion imaging with SPECT and SPECT/CT: 2015 revision. **Eur J Nucl Med Mol Imaging 42 (2015)1929–1940.**
7. Ishihara, M., Taniguchi, Y., Onoguchi, M., Shilbutani, T., Optimal thallium-201 dose in cadmium-zinc-telluride SPECT myocardial perfusion imaging. **J. Nucl Cardiol. 25 (2016) 947–954.**
8. Songy, B., Lussato, D., Guernou, M., Queneau, M., Gerraonazo, R. Comparison of myocardial perfusion imaging using thallium-201 between a new cadmium-zinc-telluride cardiac camera and a conventional SPECT camera. **Clin. Nucl. Med. 36 (2011) 776-780.**
9. Henzlova, M.J., Duvall, W.L. Tl-201 dosing for CZT SPECT: More new Information. **J. Nucl Cardiol. 25 (2018) 955–957.**
10. IAEA Radioisotopes and Radiopharmaceuticals No 2, 2017. Cyclotron Based Production Technetium-99m. INTERNATIONAL ATOMIC ENERGY AGENCY, Vienna.
11. Mitra, A., Chattopadhyay, S., Chandak, A., Lad, S., Barua, L., De A., Kumar, U., Chinagandham, R., Upadhye, T., Koundal, K., Banerjee, S., Rajan, R., Clinical Efficacy of

Sodium [^{99m}Tc] Pertechnetate from Low Specific Activity ^{99}Mo/^{99m}Tc Autosolex Generator in Hospital Radiopharmacy Center. **Nucl. Med. Rev. 23 (2020) 1-13.**

12. Underwood, S. R., Wiener, S. Myocardial perfusion scintigraphy in Europe 2005: A survey of the European Council on Nuclear Cardiology. **Eur. J. Nucl. Med. Mol. Imaging 36 (2009) 260–268.**

13. Qaim, S.M., Weinreich, R., Ollig, H. Production of ^{201}Tl and ^{203}Pb via proton induced nuclear reactions on natural thallium, Int. **J. Appl. Radiat. Isot. 30 (1979) 85–95.**

14. Britto, J.L.Q., Braghirolli, A.M.S., Silva, A.G. A new production method for carrier-free ^{201}Tl using IEN's cyclotron in Rio De Janeiro. **J. Radioanal. Nucl. Chem. 96 (1985).181–186.**

15. Lebowitz, E., Greene M. W., Fairchild, R., Bradley-Moore, P. R., Atkins, H. L., Ansari, A. N., Richards, P., Belgrave E., 1975. Thallium-201 for medical use. **J. Nucl. Med. 16 (1975) 151–155.**

16. Manual Tl-201 Production Process at DAE Medical Cyclotron Facility Kolkata, VUB, Brussels, Belgium, 16 May, 2008.

17. Sarzanini, C., Sacchero, G., Mentasti, E., Hajo´s P. Studies on the retention behavior of metal-EDTA complexes in cation chromatography. **J. Chromatogr. A 706 (1995) 141-147.**

18. Trtić, T. M., Vladisavljević, G.T., Čomor. J. J., Dispersion-Free Solvent Extraction of Thallium (III) in Hollow Fiber Contactors. **Sep. Sci. Technol. 35/10 (2000) 1587-1601.**

19. Deptula, Cz., Zaitseva, N. G., Mikolayewsky, S., Khalkin, V. A., Sorption technique of separation of thallium-201 from proton-irradiated thallium. **Isotopenpraxis, 26/10 (1990) 476-479.**

20. Rösch, F., Hung, T. K., Milanov, M., Khalkin, V. A. Electromigration of carrier-free radionuclides. 7. ^{201}Tl-Thallium (I) sulphate complexes in aqueous solutions. **Isotopenpraxis 24/10 (1888) 386-388.**

21. Trtić T.M. and Čomor, J. J. Extraction of thallium with butyl acetate, **Sep. Sci. Technol. 34/5 (1999) 771-779.**

22. Sodd, V. J., Scholz, K. L., Blue, J. W. Separation of thallium-201 from lead-201 using n-benzylaniline. **J. Radioanal. Chem. 68/1-2 (1982) 277-280.**

23. Nikjou, A., Sadeghi, M., Azizakram, H. ^{201}Tl production through light charged-particle induced reactions on Tl and Hg isotopes: theoretical and simulation approaches, **J. Radioanal. Nucl. Chem. 319 (2019) 61–68.**

24. Dutta, B., Maiti, M., Lahiri, S. Production and separation of no-carrier-added thallium isotopes from proton irradiated $^{nat}Hg_2Cl_2$ matrix. **Appl. Radiat. Isot. 69/10 (2011) 1337-1342.**

25. United States Pharmacopeia 43rd / The National Formulary 38th, (2019). Thallous Chloride Tl 201 Injection, p. 4318.

26. European Pharmacopoeia 9.0, Thallous (^{201}Tl) Chloride Injection. **Monograph 01/2008:0571 (2020) 1202.**

27. International Pharmacopoeia 4th, Thallous (^{201}Tl) Chloride Injection. **Monograph QAS/13.549/Rev. 2 (2014) p. 2.**

28. Romanelli, L., Evandri, M.G. Permitted daily exposure for diisopropyl ether as a residual solvent in pharmaceuticals. **Toxicol. Res. 34 (2018) 111–125.**

29. Vander Walt, T.N., Naidoo, C. Recovery of ^{201}Tl by ion exchange chromatography from proton bombarded thallium cyclotron targets. **Radiochim. Acta 88 (2000) 185-187.**

30. Staelens, S.G., deWit, T.C., Lemahieu, I.A., Beekman, J.F. Degradation of myocardial perfusion SPECT images caused by contaminants in thallous (^{201}Tl) chloride. **Eur. J. Nucl Med. Mol. Imaging. 35 (2008) 922-932.**

31. Sattari, A., Aslani, G., Dehghan, M.K., Shirazi, B., Shafie, M., Shadanpour, N., Winkel, P.V. Dependence of quality of thallium-201 on irradiation data. **Iran. J. Radiat. Res. 1 (2003) 51-54.**

Temperature Profile of MTP-1200 Package for Normal Conditions of Transport

Prashant Dewan, Mukhar Sharma, Dhiren Sahoo

Radiation Technology Development (RTD), BRIT

prashant.dewan@britatom.gov.in

Abstract

BRIT has set up a Fission Molybdenum-99 Production (FMP) facility at BARC Trombay, while preparation of column generator facility is at Navi Mumbai. The MTP-1200 package shall be used for transportation of high specific activity ^{99}Mo from FMP. The decay of ^{99}Mo produces ^{99m}Tc which is used in diagnostic scans. The timelines of producing technetium generators and delivering them to diagnostic centres is tightly scheduled and highly time dependent. The MTP container is designed as a Type B(U) package having a source capacity of 44.4 TBq (1200 curies) of ^{99}Mo. The shielding material used in the package is tungsten alloy encased in steel lining. The use of tungsten as shielding material results in compact and lightweight design. As per AERB and IAEA guidelines the container has to demonstrate its thermal conformance under normal transport conditions and hypothetical accident conditions to qualify as a Type B (U) package.

Introduction

The MTP-1200 cask is shown in Fig. 1. The product bottle containing ^{99}Mo as sodium molybdate in liquid solution form is placed in source housing. The source housing is placed in cask source cavity and shield plug is bolted to cask body. The shield plug has 3 nos. perfluoroelastomer 'O' ring gaskets which ensures leak tightness of the containment. The package uses tungsten as shielding material for compact and lightweight design. The total weight of unit with over-pack is approximately 225 kg. The tungsten shielding is enclosed within SS304L lining. The cask is enclosed in an over-pack. The over-pack has SS304L lined high density polyurethane foam (PUF) which acts as safety barrier in hypothetical accident conditions. The outer dimensions of the package are 390 mm diameter and 520 mm height. It is envisaged that PUF will protect the cask in hypothetical fire accident conditions. It is expected that over-pack will withstand full impact of fire while insulating the cask and in doing so the over-pack will get severely damaged in hypothetical fire accident condition. The AERB/IAEA guidelines mandates an accessible surface temperature of 50°C for type B(U) package.

Simulation procedure

A general-purpose finite element (FE) heat transfer code was used for thermal analysis of cask. The multipurpose code allows performing two- and three-dimensional modelling using FE method. An axi-symmetric model of cask has been considered for finite element simulation. The model of cask is shown in Fig. 2. The accessories of mechanisms, gaskets, wooden base, bolts and lifting lugs have

been neglected. The total heat generated in cask due to radioactive decay of 1200 Ci ^{99}Mo source is 4.9 W, it is applied in terms of average heat flux on product bottle. The decay heat is applied with time dependent radioactive decay of ^{99}Mo. The predominant thermal source is ^{99}Mo, contributing 82% to the thermal power, whereas ^{99m}Tc contributes the remainder. The payload's initial thermal power decays rapidly due to short half-lives of these two contributors. The half-lives of ^{99}Mo and ^{99m}Tc are 66 hours and 6 hours approximately. The product bottle is assumed to absorb 82% of the source thermal power whereas rest is absorbed by cask inner cavity. The convection within air gaps of package is neglected however air conduction is considered using gap conductance. The surface heat flux of package is small enough for heat to be dissipated by surface conduction alone. A nominal convection coefficient and surface radiation has been used in simulation. The heat flow in package is described by following equations:

$$\nabla^2 T + \frac{\dot{q}}{k} = \frac{1}{\alpha}\frac{\partial T}{\partial t}$$

$$Q_{conv} = hA(T_{cask} - T_a)$$

$$Q_{rad} = \sigma \varepsilon A\left(T_{cask}^4 - T_a^4\right)$$

The first equation represents heat conduction through package whereas other equations represent heat loss from package exterior surfaces.

h- average heat transfer coefficient; $Tcask$- average surface temperature of cask; $\dot{q}$– volumetric heat release in package; k– thermal conductivity of package material; α- thermal diffusivity; $Qconv$- heat loss by convection; $Qrad$– heat loss by radiation ;A– outer surface area of package; σ- Stefan-Boltzmann constant; ε – emissivity of cask; Ta- reference ambient temperature 38°C as per IAEA recommendations (Regulations,

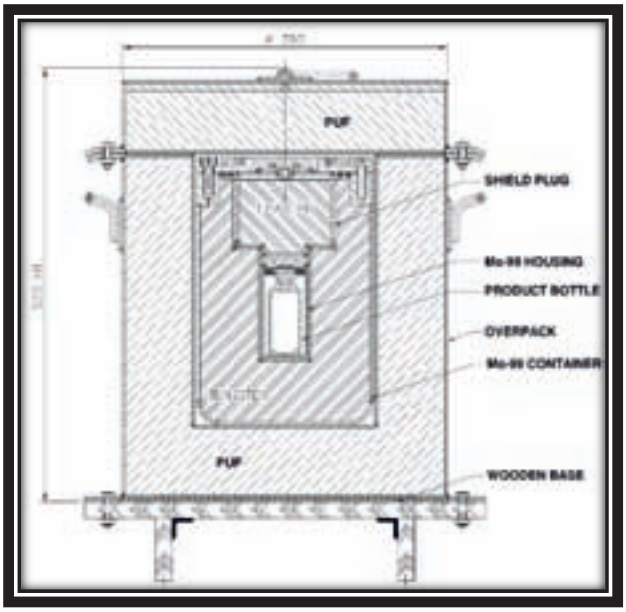

Fig. 1 Cross sectional elevation of package

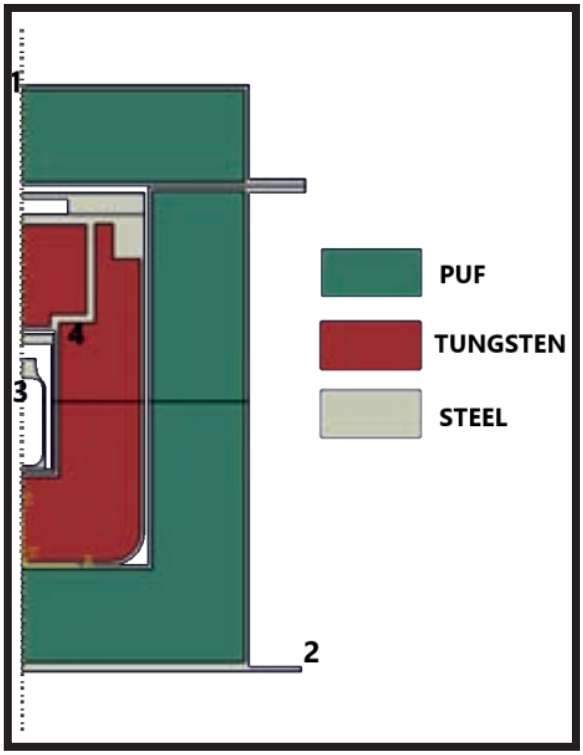

Fig. 2 Axi-symmetric model of package

2018). The solar insolation specified by IAEA recommendations with 12-hour diurnal insolation cycle (Regulations, 2018) is 800W/m^2 at top surface, 200 W/m^2 at vertical package surfaces and 400 W/m^2 at other exposed surfaces of package (excluding package bottom). An emissivity of 0.3 and solar absorptivity of 0.52 and is considered for package exterior surface.

The thermal conductivity of steel and tungsten is shown in Table 1 and Table 2 respectively, whereas, other physical properties of materials are shown in Table 3.

Table 1. Thermal conductivity of steel

Thermal Conductivity (W/mK)	Temp. (°C)
14.8	30
15.9	100
17.4	200

Table 2. Thermal conductivity of tungsten

Thermal Conductivity (W/mK)	Temp. (°C)
174	30
163	100
152	200

Table 3. Properties of various materials

Sr. no.	Material	Density (kg/m^3)	Specific heat (J/kgK)
1	Stainless steel	8,000	460
2	Tungsten	19,000	130
3	Polyurethane foam	400	1,288

Results and discussion

The temperature contour of Mo-99 package under normal condition of transport without and with solar insolation is presented in Fig. 3. The maximum accessible temperature of package without solar insolation is 38.5°C. As shown in Fig. 3 the maximum temperature of bottle carrying molybdenum without and with solar insolation is 59.61°C and 70.45°C respectively.

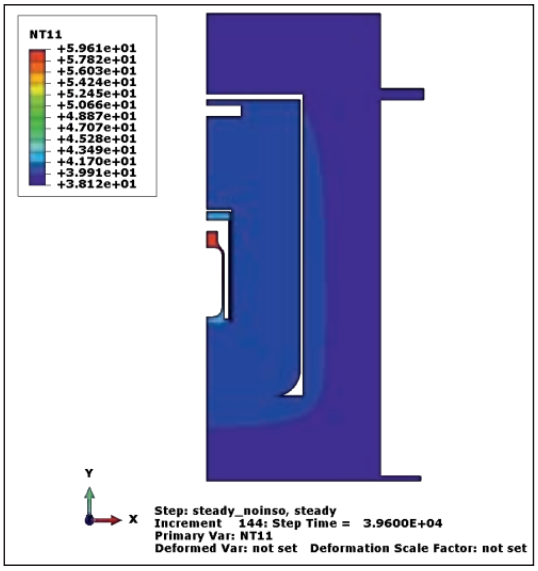

Fig. 3a: Normal condition temperature distribution in package without solar flux at time of peak payload temperature (11 hrs after loading)

Fig. 4 illustrates the predicted transient thermal response of the package for normal condition of transport with solar insolation. The effect of the diurnal insolation cycle can be seen in the temperature response of the over-pack base and lid. The initial portion of the temperature response for the cask seal is dominated by the initial heat-up of the cask, while the later portion of the response reflects the influence of the diurnal insolation cycling. The transient demonstrates that peak cask temperature is achieved in 37.5 hours. After that time point, the decreasing source decay heat load results in ever lower package temperatures.

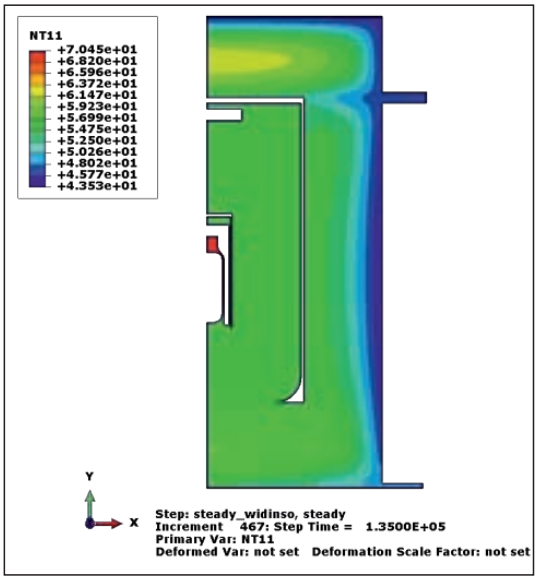

Fig. 3b: Normal condition temperature distribution in package with solar flux at time of peak payload temperature (37.5 hrs after loading)

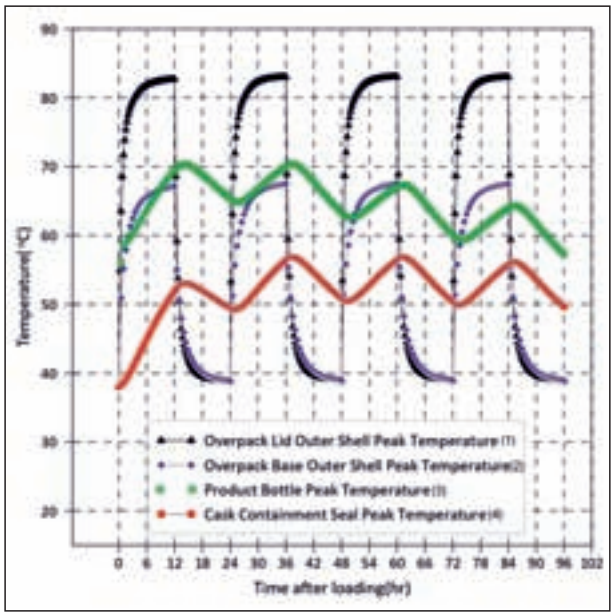

Fig. 4 Normal condition of transport with solar insolation transient results

Conclusion

In this study thermal simulation of MTP-1200 cask for normal conditions of transport was carried out according to IAEA/AERB regulations. The hypothetical accident pool fire condition was not simulated as the cask is enclosed in protective PUF enclosure and damage to cask during accident fire conditions is not envisaged. As such the study signifies that package fulfils the thermal requirements of safety for normal conditions of transport.

References

1. IAEA safety standards no. SSR-6 (Rev. 1) "Regulations for the Safe Transport of Radioactive Material", **(2018)** edition.
2. IAEA safety standards series safety guide no. SSG-26 "Advisory Material for the IAEA regulation for the Safe Transport of Radioactive Material" **(2018)** edition.
3. John H. Lienhard IV and V, "A heat transfer textbook" Third edition, Phlogiston press **(2006)**.
4. R. Poskas, V. Simonis, P. Poskas, A. Sirvydas, "Thermal analysis of castor RBMK-1500 casks during long-term storage of spent nuclear fuel". **Annals of Nuclear Energy 99 (2017) 40-46.**
5. Jie Li, Yung Y. Liu, "Thermal modeling of a vertical dry storage cask for used nuclear fuel", **Nuclear Engineering and Design 301 (2016) 74-88.**
6. G. Pugliese, R. Lo Frano, G. Forasassi, "Spent fuel transportation cask thermal evaluation under normal and accident conditions". **Nuclear Engineering and Design 240 (2010) 1699-1706.**

Development of ^{68}Ga-Based Lyophilized Kit Formulation Towards PET Imaging of Tumor-Induced Angiogenesis

Soumen Das,[1,2] Avik Chakraborty,[2,3] Rubel Chakravarty,[2,4] Sudipta Chakraborty[2,4]*

[1]Radiopharmaceuticals Program, BRIT, [2]Homi Bhabha National Institute, [3]Radiation Medicine Centre, BARC, [4]Radiopharmaceuticals Division, BARC

email: soumen.das@britatom.gov.in

Abstract

Radiolabeled Arg-Gly-Asp (RGD) peptide derivatives have already proven themselves to be an important marker for the non-invasive monitoring of integrin $\alpha_v\beta_3$ receptors over-expressed by several malignancies during the 'angiogenic switch'. Hence, availability of a suitable radiotracer via a lyophilized kit formulation would ensure round-the-clock availability in a hospital radiopharmacy set-up and would facilitate proper clinical management of these life-threatening conditions. Towards this, the present article describes the development of a lyophilized kit formulation for the preparation of clinical doses of [^{68}Ga]Ga-DOTA-E[c(RGDfK)]$_2$ (E = glutamic acid, f = phenylalanine, K = lysine) radiotracer towards PET imaging of tumor-induced angiogenesis.

The kit was formulated under aseptic conditions inside a Class 100 clean room with optimized kit contents and lyophilized for 24 hours. On radiolabeling with [^{68}Ga]$GaCl_3$, the radiotracer was found to be formed with high radiolabeling yield (>90%) and high radiochemical purity (>95%). *In-vivo* biodistribution studies with the radiotracer prepared from the kit formulation carried out in melanoma tumour-bearing SCID mice exhibited significant accumulation of the radiotracer in the tumor xenograft (>5%) at 1-hour post-injection. All these results point towards the promising attributes of the developed kit formulation and warrant further clinical investigation.

Introduction

Cancer currently ranks as the second leading cause of death worldwide after coronary artery diseases with an estimated 19.3 million new cancer cases and almost 10 million cancer deaths in 2020[1]. In fact, it is now considered to be the single most important barrier to increasing life expectancy throughout the world as according to estimates from the World Health Organization (WHO) in 2015, cancer is the first or second leading cause of death before the age of 70 years in 91 of 172 countries, and it ranks third or fourth in an additional 22 countries[2]. India ranked third after China and the United States of America for the year 2022 with an estimated number of nearly 1.46 million incident cases of cancer (about 1 in 1000 of total population) and this number is only projected to increase in the coming decades, amounting to a rise of ~57.5 per cent in 2040 from 2020[3]. However, the silver lining is that early detection of

malignancies significantly enhances the chance of survival in cancer patients.

In vertebrates, generally no cell resides beyond 50-100 μm distance from a capillary. Oxygen is generally diffused from the bloodstream to the cell area but since the diffusion capacity is limited there exists a gradient. As a result, the cells of both the primary and the secondary tumor mass starts to grow and a lack of oxygen and nutrients arise towards the centre. The peripheral tumor cells which are in close proximity to the blood vessel get sufficient oxygen and nutrients while the cells in the centre which fall beyond the normal diffusion capacity become necrotic or even apoptotic. Thus, in the absence of vascular support the size of tumors is naturally limited to 1-2 mm^3 ($\sim 10^6$ cells). In response to this hypoxic micro-environment, tumors start to up-regulate growth factors that facilitate a process termed as 'angiogenesis', which denotes the process of formation of new blood vessels from pre-existing ones through the *de-novo* production of endothelial cells.

In most mature adult tissues, the rate of proliferation of endothelial cells is very low compared with that of many other cell types in the body, except in the female reproductive system and during wound healing. Under normal physiological conditions, endothelial cells remain in a dormant state as the delicate balance between pro-angiogenic factors (VEGF, angiopoietins, bFGF) and anti-angiogenic factors (thrombospondins, angiostatin and endostatin) is maintained. However, this balance is frequently tilted towards angiogenesis inducers (and simultaneously offsetting inhibitors) by tumors which by virtue of accrued mutations starts to release growth factors like VEGF and this affects the existing blood vessels and turns on the so-called 'angiogenic switch'[4]. Once this happens, the tumor starts to grow rapidly and its volume starts to increase in an exponential manner. This

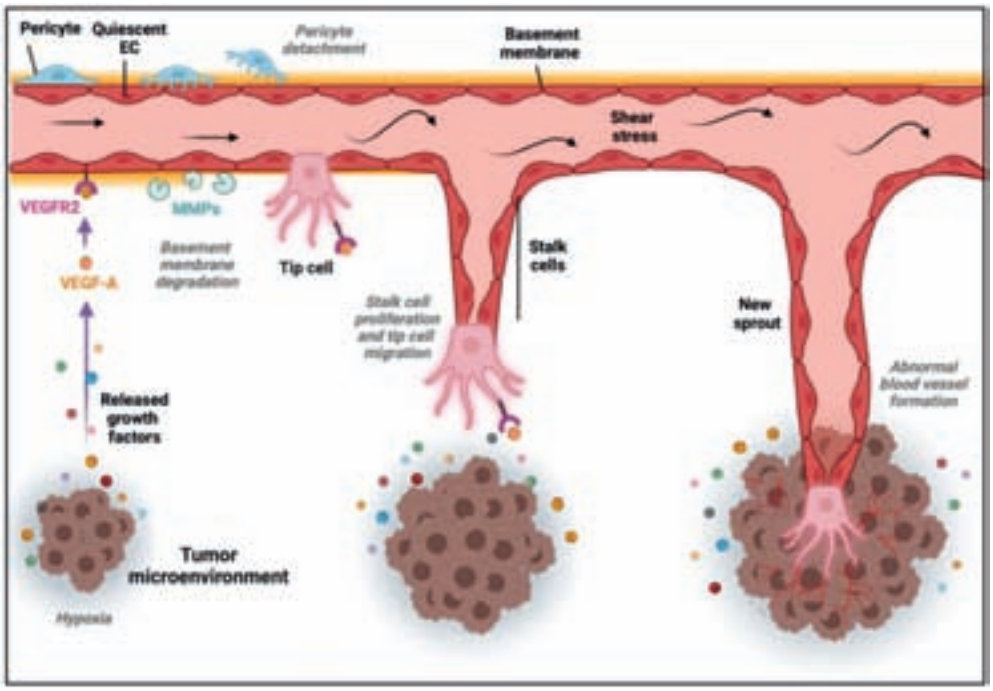

Fig. 1: Tumor growth and angiogenic switch[4]

pathological angiogenesis process not only ensures a sustained supply of additional nourishment to the proliferating tumor cells but also helps in removing CO_2 and toxic metabolic waste and provides a route for tumor cells to metastasize further. Therefore, non-invasive imaging of tumor-induced angiogenesis could potentially be utilized for early diagnosis of malignancies, monitoring tumor progression and planning as well as evaluating the efficacy of therapeutic regimen. It could also be fruitful in the development of emerging treatment modalities like anti-angiogenic therapy, which is aimed at 'starving' the tumor, with monoclonal antibodies like bevacizumab and synthetic peptides like cilengitide.

Adhesion molecules play an extremely crucial role in the angiogenic process by providing the traction necessary for vascular endothelial cell migration and regulating local invasion. Integrins, the main cell adhesion receptors, are a family composed of 24 unique heterodimeric transmembrane glycoproteins in mammals that are generated from a combination of eighteen α and eight β sub-units and are essential in the migration, invasion, proliferation, survival and metastatic spread of neoplastic cells. These receptors directly bind components of the extracellular matrix, such as fibronectin, vitronectin, laminin or collagen and provide anchorage for cell motility and invasion. One among these receptors, viz. integrin $\alpha_v\beta_3$ plays a pivotal role in the whole process and is found to be over-expressed on the proliferating endothelial cells associated with the neovasculature of tumors and correlate well with tumor progression and invasiveness of several malignancies like melanoma, glioma, osteosarcomas, neuroblastomas, lung carcinomas, ovarian and breast cancer [5-15]. As these receptors are known to bind to extracellular matrix proteins presenting the exposed arginine-glycine-aspartic acid (RGD) tripeptide sequence, linear as well as cyclic synthetic peptides based on the above-specified tripeptide sequence could serve as radioisotope delivery vehicles for these molecular targets and thereby facilitating non-invasive monitoring of primary as well as metastatic tumors by SPECT or PET [5,7,16,17].

Over the last two decades, a large number of radiolabeled RGD-based peptide derivatives have been synthesized and investigated as potent antagonists for imaging integrin $\alpha_v\beta_3$ expression in various tumor types by SPECT or PET[7,9,21-26]. In this context, a cyclic pentapeptide dimer $E[c(RGDfK)]_2$ (E = glutamic acid, R = arginine, G = glycine, D = aspartic acid, f = phenylalanine, K = lysine) has shown high promise as the integrin $\alpha_v\beta_3$ receptor targeting vector [7, 17, 28, 31-34]. Hence, there is an ongoing need for ^{99m}Tc/^{68}Ga-labeled radiotracers based on this peptide that can be readily prepared at hospital radiopharmacy set-ups and used without any post-labeling purification. As the current routine practice for these two relatively short-lived radioisotopes ($t_{1/2}$ for ^{99m}Tc: 6 hr and for ^{68}Ga: 68 min) is mainly driven by in-house radiolabeling of lyophilized kits using the ^{99m}Tc/^{68}Ga-activity eluted from commercial generators in a hospital radiopharmacy set-up, the availability of robust kit formulations for convenient one-step preparation of suitable radiotracers for clinical applications would be really beneficial for nuclear medicine facilities with high footfall. This would augment the utility of this class of molecular imaging

agents and at the same time would be cost-effective also since a number of patient doses may be obtained from a single multi-dose vial.

Against this backdrop, a ^{99m}Tc-based kit for the preparation of [^{99m}Tc]Tc-HYNIC-E[c(RGDfK)]$_2$ was developed recently which has already become a part of the product catalogue of BRIT under the code name TCK 59 [29]. Herein, we describe the formulation and pre-clinical evaluation of a lyophilized kit formulation for the rapid and convenient preparation of [^{68}Ga]Ga-DOTA-E[c(RGDfK)]$_2$ radiotracer at the hospital end for routine clinical application in tumor-induced angiogenesis imaging.

Experimental

Materials and methods

DOTA-E[c(RGDfK)]$_2$ peptide conjugate with purity in excess of 98% was purchased from M/s ABX Biochemicals, Radeberg, Germany. Suprapure sodium acetate (metal trace grade) was obtained from Merck, India. Ultrapure (Type 1) water used in the formulations was obtained from Milli Q system (18.2 MΩ) available from M/s Millipore, India. Sterile filtration of solutions was carried out using Millex-GP membrane filters (0.22 µm) procured from Merck Millipore, Germany. Lyophilization was carried out in a general purpose lyophilizer (Martin Chirst, Germany, Model: Epsilon 2-25 D). Sterility of the lyophilized kits was tested in tryptic soy broth media and fluid thioglycolate media using sterility test kits obtained from HiMedia Laboratories, India. Bacterial endotoxin test was carried out using Endosafe nexgen-PTS equipment and cartridges for endotoxin detection (sensitivity: 0.50-0.05 EU/mL), procured from Charles River, USA.

Gallium-68 activity was obtained in the form of [^{68}Ga]GaCl$_3$ by eluting a 1.85 GBq (50mCi) ^{68}Ge-^{68}Ga generator (ITG, Germany) with 0.05 M suprapure HCl. Silica gel plates used for performing TLC were obtained from Merck, India. HPLC analyses of [^{68}Ga]Ga-DOTA-E[c(RGDfK)]$_2$ radiotracer were performed using a JASCO PU 2080 Plus dual pump HPLC system, Japan, with a JASCO 2075 Plus tunable absorption detector and Gina Star radioactivity detector system, using a C18 reversed-phase HiQ Sil (5 µm, 4 × 250 mm) column.

Standardization of kit components

Sodium acetate content was standardized at by studying the effect of its concentration (0.2-0.5 M) on the pH of the final solution after the addition of 4 mL of 0.05 M or 0.1 M suprapure HCl. Peptide content in each kit vial was optimized based on the results of radiochemical studies with varying amount of peptide (15-35 µg) for obtaining >90% yield of [^{68}Ga]Ga-DOTA-E[c(RGDfK)]$_2$ under previously standardized reaction conditions for ^{68}Ga-DOTA labeling[30].

Formulation and quality control of lyophilized DOTA-E[c(RGDfK)]$_2$ kits

The typical protocol followed during the formulation of a batch of 25 vials of lyophilized DOTA-E[c(RGDfK)]$_2$ kit is described here. The procedure was carried out under aseptic conditions in a Class 100 clean room facility. 925 mg of sodium acetate was dissolved in 20 mL of ultrapure water and then 500 µg of DOTA-E[c(RGDfK)]$_2$ peptide, separately dissolved in 2 mL of ultrapure water, was added to this solution. The final volume was made up to 25 mL by adding further 3 mL of ultrapure water. The solution was then

sterilized by passing through a 0.22 µm membrane filter assembly. From the bulk solution 1 mL each was dispensed in 10 mL sterile glass vials which were then partially closed with sterile slotted rubber closures and the contents were then lyophilized for 24 h. The lyophilized vials were sealed under nitrogen and stored at -20°C till further use. Three different batches of the kit were prepared following this protocol.

Kits were tested for sterility and apyrogenicity using the standard procedure. From each batch, kit vials were randomly picked and kit components were dissolved in 1 mL of sterile ultrapure water and the tests were conducted.

Preparation of [^{68}Ga]Ga-DOTA-E[c(RGDfK)]$_2$ using lyophilized kits

The kit vials were reconstituted with 1 mL of ultrapure water and 1 mL of air was removed. Then ~4 mL of [^{68}Ga]$GaCl_3$ (222-296 MBq) in 0.05 M HCl, freshly eluted from a commercial ^{68}Ge-^{68}Ga generator (Make: ITG), was added to the vial and heated at 100°C for 15 min. The contents of the vial were then cooled to room temperature and quality control tests were conducted.

Determination of radiochemical purity of [^{68}Ga]Ga-DOTA-E[c(RGDfK)]$_2$

Radiochemical purity of the radiotracer was determined through radio-TLC and radio-HPLC methods. In radio-TLC, 0.1 M citrate buffer (pH 4.5) was used as the mobile phase, while, in radio-HPLC, water (A) and acetonitrile (B) mixtures with 0.1% trifluoroacetic acid were used. The gradient elution technique adopted was 0-4 min 95% A, 4-15 min 95% A to 5% A, 15-20 min 5% A, 20-25 min 5% A to 95% A, 25-30 min 95% A. Flow rate was maintained at 1 mL/min. About 10 µL aliquot of the radiolabeled preparation was injected into the HPLC column and the radioactive elution profile was followed for the identification of different radiochemical species likely to be present.

Pre-clinical investigation of [^{68}Ga]Ga-DOTA-E[c(RGDfK)]$_2$

Evaluation of *in-vivo* localization of the radiopharmaceutical was carried out by performing biodistribution study in 3 to 4 weeks old female SCID mice (20-25 g) bearing melanoma tumors, which are known to over-express integrin $\alpha_v\beta_3$ receptors. Mice were injected subcutaneously into the right thigh with melanoma cancer cells (1×10^6 cells/mice) and the xenografts were allowed to grow for 2 to 3 weeks until the tumor reached the required size (~1-1.5 cm^3 volume). On the day of the experiment, mice were injected with freshly prepared [^{68}Ga]Ga-DOTA-E[c(RGDfK)]$_2$ (3.0-3.7 MBq/animal, 100 μL) through the tail vein under isoflurane-oxygen anesthesia. Respective animals (n = 3) were sacrificed by CO_2 asphyxiation at the end of 30 minutes and 1-hour post-injection (p.i.). Various organs, tissues and tumors were then excised and the radioactivity associated with each was measured using a flat-bed type NaI(Tl) counter.

Results and Discussion

Reaction pH has been observed to have a profound influence on ^{68}Ga-labeling, with the optimum pH being in the range of 3 to 4. This is achieved by using sodium acetate as a kit component which is known to have a buffering action after the addition of acids. Currently available commercial ^{68}Ge-^{68}Ga generators differ in the HCl eluate volume and molarity

depending on the different column matrix being used and thus the sodium acetate content in the kit becomes really important as insufficient buffer quantity during radiolabeling will inevitably lead to lower radiolabeling yield and radiochemical purity. The two most popular commercial generators, being supplied by ITG Isotope Technologies (Munchen, Germany) and Eckert & Ziegler (Germany), employ 0.05 M and 0.1 M HCl respectively for eluting the ^{68}Ga-activity. Hence, in the present work, the sodium acetate content in the kit vial was standardized in such a way that the same kit formulation can be used for both the generators. This was done by adding sodium acetate solution of different concentrations (0.25, 0.30, 0.35, 0.40 and 0.45 M) to 4 mL (approximate eluate volume) of either 0.05 M or 0.01 M suprapure HCl and then measuring the pH. From this study, 0.45 M resulted as the optimum sodium acetate concentration as it was observed that 1 mL of this solution could automatically adjust the pH of the final solution to ~3.5 in both the cases. Lower concentrations required higher volume of sodium acetate solution to perform the buffering action in the case of 0.1 M HCl which could prove to be detrimental with respect to the radiolabeling yield due to the increase in reaction volume (>5 mL).

The peptide content present per kit vial is also a very important parameter since presence of excess cold peptide will lead to a competition between the radiolabeled and unlabeled peptide molecules for the finite number of cell-surface receptors available for binding and might also lead to a saturation of the receptor sites. This was standardized by heating freshly eluted [^{68}Ga]$GaCl_3$ (~5 mCi in ~4 mL of 0.05 M HCl) with varying amount (in the range of 15-35 μg) of DOTA-E[c(RGDfK)]$_2$ (in 1 mL of 0.45 M sodium acetate) at 100°C and then purifying the bulk solution through a C-18 cartridge to obtain the radiolabeling yields. From this set of analysis, it was found that 20 μg of peptide per vial was most suitable for kit formulation purpose.

Three batches of the newly formulated DOTA-E[c(RGDfK)]$_2$ kit was prepared with the standardized kit contents following the procedure specified and thoroughly tested for all the necessary physicochemical parameters like appearance, pH, radiochemical purity and biological parameters like sterility and apyrogenicity to ensure the reproducibility of the formulation and its suitability for clinical use.

Radiochemical purity of the [^{68}Ga]Ga-DOTA-E[c(RGDfK)]$_2$ radiotracer prepared from the lyophilized kits was found to be >95% for all the prepared batches as per

Table 1 Standardization of sodium acetate content per kit vial

Concentration of HCl	Required volume of sodium acetate solutions of a particular concentration to adjust the pH of HCl to ~3.5				
	0.25 M	0.30 M	0.35 M	0.40 M	0.45 M
0.05 N	1.1 mL	1 mL	1 mL	0.8 mL	0.5 mL
0.1 N	1.7 mL	1.5 mL	1.5 mL	1.3 mL	1 mL

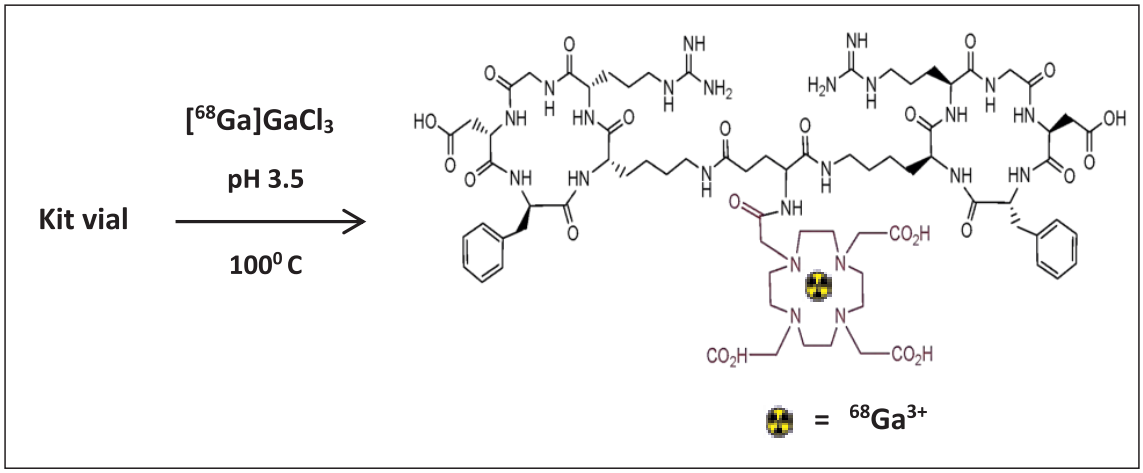

Fig. 2: Schematic representation of the formulation of [^{68}Ga]Ga-DOTA-E[c(RGDfK)]$_2$ radiotracer from lyophilized kit vials for clinical use

Table 2 Variation of radiolabeling yield with peptide content

Peptide content (μg)	%Radiolabeling yield
15	89.82 ± 0.23
20	91.09 ± 0.41
25	93.51 ± 0.53
30	94.23 ± 0.32
35	95.16 ± 0.15

radio-TLC. This was further corroborated by the radio-HPLC profile which exhibited a major peak corresponding to the radiotracer at 16.2 min, while <5% (decay corrected) unlabeled [^{68}Ga]GaCl$_3$ was eluted within 3.4 min (**Fig. 3**). Moreover, the UV-Vis HPLC profile of the labeled formulation did not exhibit any peak that could be attributed to unlabeled DOTA-E[c(RGDfK)]$_2$ or any of its radiolytic degradation product.

In-vivo biodistribution studies performed in female SCID mice xenografted with melanoma cancer cell line showed significant accumulation (5.62 ± 0.54% ID/g) of the radiotracer in the tumor along with the kidneys and bladder (10.16 ± 0.23% ID/g) at 60 min post-administration (p.i.) of ~3.7 MBq of freshly prepared [^{68}Ga]Ga-DOTA-E[c(RGDfK)]$_2$ formulation. This confirms target-specific accumulation of the radiotracer along with fast clearance of residual activity through renal route (**Fig. 4**). At the same time the activity associated with various non-target organs like liver (1.12 ± 0.18% ID/g), GIT (1.28 ± 0.23% ID/g) and lung (1.55 ± 0.32% ID/g) were found to be moderate.

Table 3 Quality control of [^{68}Ga]Ga-DOTA-E[c(RGDfK)]$_2$ prepared using different batches of lyophilized kits

Quality control parameter	Test method	Desired results	Results obtained		
			B-1	B-2	B-3
Appearance	Visual inspection	Clear, colorless solution	As desired	As desired	As desired
pH	Non-bleeding pH paper	3-4	3.5	3.5	4.0
% RCP	Radio-TLC	>95%	98.85 ± 0.40	98.29 ± 0.38	99.08 ± 0.15
	Radio-HPLC		98.61 ± 0.32	97.43 ± 0.56	98.59 ± 0.31
Sterility	Media incubation	Should be sterile	Sterile	sterile	Sterile
Bacterial endotoxin	LAL test	<25 EU/mL	Passed	Passed	Passed

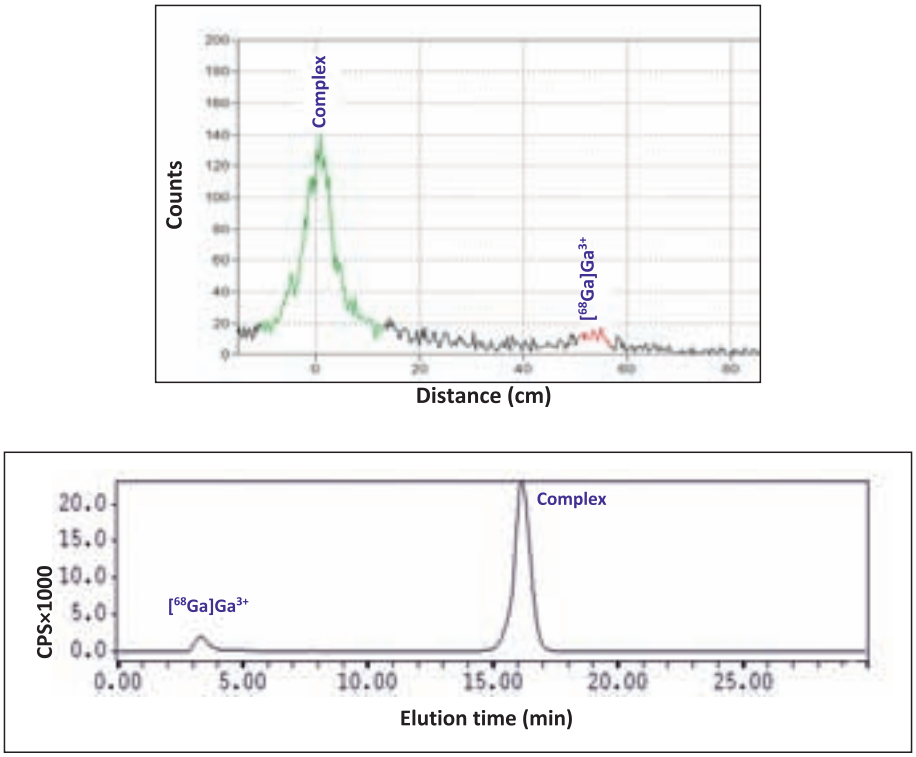

Fig. 3: Representative radio-TLC and radio-HPLC patterns of [^{68}Ga]Ga-DOTA-E[c(RGDfK)]$_2$ radiotracer formulation prepared from the lyophilized DOTA-E[c(RGDfK)]$_2$ kits indicating high radiochemical purity of the formulation

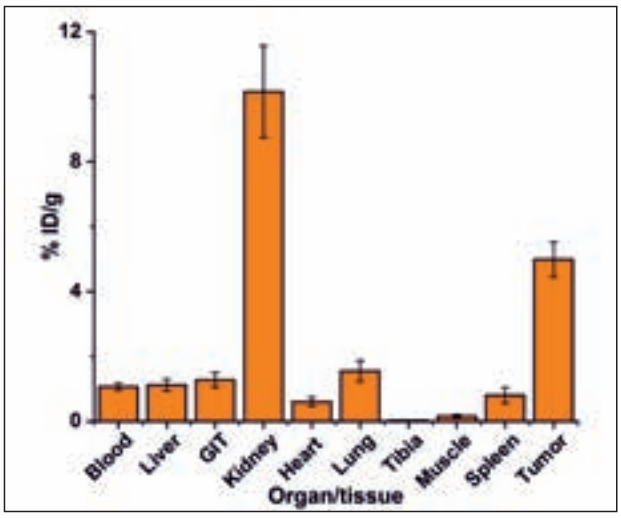

Fig. 4: *In-vivo* **biodistribution pattern of [^{68}Ga]Ga-DOTA-E[c(RGDfK)]2 formulation in SCID mice xenografted with FTC133 human thyroid cancer cell line**

Conclusion

A lyophilized kit for the convenient one-pot formulation of [^{68}Ga]Ga-DOTA-E[c(RGDfK)]$_2$ for routine clinical use in PET imaging of tumor-induced angiogenesis was developed. Using this kit, the radiotracer could be successfully prepared with excellent radiochemical purity (>98%) and high specific activity (~15.8 GBq/μmol) following a procedure which can be easily adopted even in a busy hospital radiopharmacy set-up. *In-vivo* biodistribution studies in melanoma tumor-bearing female SCID mice showed significant accumulation of the radiotracer in the tumor at 60 min p.i. without significant uptake in major non-target organs. All these results point toward the potency of this formulation for routine clinical use in the fight against cancer.

References

1. Sung H, Ferlay J, Siegel RL, Laversanne M, Soerjomataram I, et al. Global Cancer Statistics 2020: GLOBOCAN Estimates of Incidence and Mortality Worldwide for 36 Cancers in 185 Countries. **CA: A Cancer Journal for Clinicians 71 (2021) 209-249**.
2. Bray F, Ferlay J, Soerjomataram I, Siegel RL, Torre LA, et al. **CA Cancer J Clin 68 (2018) 394-424.**
3. Sathishkumar K, Chaturvedi M, Das P, Stephen S, Mathur P. Cancer incidence estimates for 2022 & projection for 2025: Result from National Cancer Registry Programme, India. **Indian Journal of Medical Research 156 (2022) 598-607**.
4. Garcia-Caballero M, Sokol L, Cuypers A, Carmeliet P. Metabolic Reprogramming in Tumor Endothelial Cells. **Int J Mol Sci 23 (2022) 11052**.
5. Hin J, Varner H. Integrins: roles in cancer development and as treatment targets. **Br J Cancer 90 (2004) 561-565.**
6. Haubner R. $\alpha_v\beta_3$-integrin -imaging: a new approach to characterise angiogenesis? **Eur J Nucl Med Mol Imaging 33 (2006) 54-63.**
7. Liu S. Radiolabeled multimeric cyclic RGD peptides as integrin $\alpha_v\beta_3$ targeted radiotracers for tumor imaging. **Mol Pharm 3 (2006) 472-487.**
8. Liu Z, Wang F, Chen X. Integrin $\alpha_v\beta_3$-targeted cancer therapy. **Drug Dev Res 69 (2008) 329-339.**
9. Cai W, Chen X. Multimodality molecular imaging of tumor angiogenesis. **J Nucl Med 49 (2008) 113S-128S.**
10. Desgrosellier JS, Cheresh DA. Integrins in cancer: biological implications and therapeutic opportunities. **Nat Rev Cancer 10 (2010) 9-22.**

11. Bello L, Francolini M, Marthyn P, Zhang J, Carroll RS, et al. $\alpha_v\beta_3$ and $\alpha_v\beta_5$ integrin expression in glioma periphery. **Neurosurgery 49 (2001) 380-389.**

12. Falcioni R, Cimino L, Gentileschi MP, D'Agnano I, Zupi G, et al. Expression of beta1, beta 3, beta 4, and beta 5 integrins by human lung carcinoma cells of different histotypes. **Exp Cell Res 210 (1994) 113-122.**

13. Landen CN, Kim T-J, Lin YG, Merritt W, Kamat AA, et al. Tumor-selective response to antibody-mediated targeting of $\alpha_v\beta_3$ integrin in ovarian cancer. **Neoplasia 10 (2008) 1259-1267.**

14. Gasparini G, Brooks PC, Biganzoli E, Vermeulen PB, Bonoldi E, et al. Vascular integrin $\alpha_v\beta_3$: a new prognostic indicator in breast cancer. **Clin Cancer Res 4 (1998) 2625-2634.**

15. Sengupta S, Chattopadhyay N, Mitra A, Ray S, Dasgupta S, et al. Role of αvβ3 integrin receptors in breast tumor. **J Exp Clin Cancer Res 20 (2001) 585-590.**

16. Kumar CC. Integrin αvβ3 as a therapeutic target for blocking tumor-induced angiogenesis. **Curr Drug Targets 4 (2003) 123-131**.

17. Danhier F, Breton AL, Preat V. RGD-based strategies to target alpha(v) beta(3) integrin in cancer therapy and diagnosis. **Mol Pharm 9 (2012) 2961-2973.**

18. Haubner R, Wester HJ, Reuning U, Senekowitsch-Schmidtke R, Diefenbach B, et al. Radiolabeled αvβ3 integrin antagonists: a new class of tracers for tumor imaging. **J Nucl Med 40 (1999) 1061-1071.**

19. Decristoforo C, Faintuch-Linkowski B, Rey A, von Guggenberg E, Rupprich M, et al. [^{99m}Tc]HYNIC-RGD for imaging integrin $\alpha_v\beta_3$ expression. **Nucl Med Biol 33 (2006) 945-952.**

20. Chen X, Park R, Tohme M, Shahinian AH, Bading JR, et al. MicroPET and autoradiographic imaging of breast cancer αv-integrin expression- using ^{18}F-and ^{64}Cu-labeled RGD peptide. **Bioconjug Chem 15 (2004) 41-49.**

21. Haubner R, Kuhnast B, Mang C. [^{18}F]Galacto-RGD: synthesis, radiolabeling, metabolic stability, and radiation dose estimates. **Bioconjug Chem 15 (2004) 61-69.**

22. Bach-Gansmo T, Danielsson R, Saracco A, Wilczek B, Bogsrud TV, et al. Integrin receptor imaging of breast cancer: a proof-of-concept study to evaluate ^{99m}Tc-NC100692. **J Nucl Med. 47 (2006) 1434-1439.**

23. Kenny LM, Coombes RC, Oulie I, Contractor KB, Miller M, et al. Phase I trial of the positron-emitting Arg-Gly-Asp (RGD) peptide radioligand 18F-AH111585 in breast cancer patients. **J Nucl Med 49 (2008) 879-886.**

24. Li ZB, Chen K, Chen X. ^{68}Ga-labeled multimeric RGD peptides for microPET imaging of integrin $\alpha_v\beta_3$ expression. **Eur J Nucl Med Mol Imaging 35 (2008) 1100-1108.**

25. Chakraborty S, Shi J, Kim Y-S, Zhou Y, Jia B, et al. Evaluation of ^{111}In-labled cyclic RGD peptides: tetrameric not tetravalent. **Bioconjug Chem 21 (2010) 969-978.**

26. Mittal S, Bhadwal M, Chakraborty S, Sarma HD, Banerjee S, et al. A novel

concept of radiosynthesis of a ^{99m}Tc-labeled dimeric RGD peptide as a potential radiotracer for tumor imaging. **Bioorg Med Chem Lett 23 (2013) 1808-1812.**

27. Janssen M, Oyen WJG, Massuger LFAG, Frielink C, Dijkgraaf I, et al. Comparison of a monomeric and dimeric radiolabeled RGD-peptide for tumor targeting. **Cancer Biother Radiopharm 17 (2002) 641-646.**

28. Dijkgraaf I, Yim C-B, Franssen GM, Schuit RC, Luurtsema G, et al. PET imaging of αvβ3 integrin expression in tumours with ^{68}Ga-labelled mono-, di- and tetrameric RGD peptides. **Eur J Nucl Med Mol Imaging 38 (2011) 128-137.**

29. Chakraborty S, Das S, Chakravarty R, Sarma HD, Vatsa R, et al. An improved kit formulation for one-pot synthesis of [^{99m}Tc]Tc-HYNIC-E[c(RGDfK)]$_2$ for routine clinical use in cancer imaging. **J Label Compd Radiopharm. 62 (2019) 823-834.**

30. Kumar D, Mathur A, Prashant V, Mirapurkar S, Das S, et al. Regular production and supply of ready-to-use gallium-68 radiopharmaceuticals: centralized radiopharmacy concept with supply experience of 300 doses. **J Radioanal Nucl Chem 330 (2021) 83-90.**

Air Conditioning and Ventilation Application for Production of Radiopharmaceuticals

Babloo Kumar[1], Chetan Kothalkar[1], Aaditya Shah[2]

[1]Medical Engineering Group (MEG), [2]Fissiaon Moly Plant (FMP)

Email: babloo.kumar@britatom.gov.in

Abstract

We often come across the terms Air Conditioning, especially in summers, and it gives us immense comfort from hot and humid atmosphere around us. So, what is this air conditioning and is there any application of this AC for production of Radiopharmaceuticals? We also come across the term AC and ventilation. So, is AC and "AC and Ventilation" the same term? We will try to learn the difference between AC and ventilation, and its application in production laboratories of Radiopharmaceuticals.

Introduction

Air Conditioning (AC) is basically controlling temperature, humidity, purity, and flow rate of air. So, we all know what temperature means, but only some has the idea about humidity. Humidity is basically measurement of water in the form of water vapour, which is present in air around us. Air present in earth atmosphere is assumed to be binary mixture of air (various gases like nitrogen, oxygen etc.) and water vapour. Humidity level must be maintained within a range. In cases when humidity goes beyond range on either side, it creates uncomfortable working conditions. Too low humidity makes air dry and makes human skin dry, whereas, too high humidity makes humans to sweat a lot. Atmospheric air present around us contains a lot of dust particles which are of various sizes, and may not be suitable for production of radiopharmaceuticals/ pharmaceuticals. Hence, filtration of this atmospheric air sometimes becomes necessary. Atmospheric air is drawn from atmosphere through a filter and further filtered through various filters in many stages to remove the dust particles. Air is filtered in successive stages to remove particles of different sizes in different stages.

Generally, any central air conditioning plants employs two types of filters i.e., coarse and fine filters for filtration of air, but facility handling production of radiopharmaceutical/ pharmaceuticals require more clean air, hence another set of filters are used for filtration of air, which is called HEPA filters. Air filtered through these filters i.e., coarse filter, fine filter and HEPA (High Efficiency Particulate Air) filter is clean enough for the laboratory for producing radiopharmaceuticals/ pharmaceuticals. There is one more category of filters, called, Ultra Low Particulate Air (ULPA) filters. These filters find application in filtration of air supplied to laboratory producing semiconductors and other sensitive electronic equipment's.

In BRIT, radiopharmaceuticals are produced, and hence, air filtered through HEPA filter is clean enough for application in the production laboratory. After filtration is complete, air is cooled by passing it through cooling coil (assembly

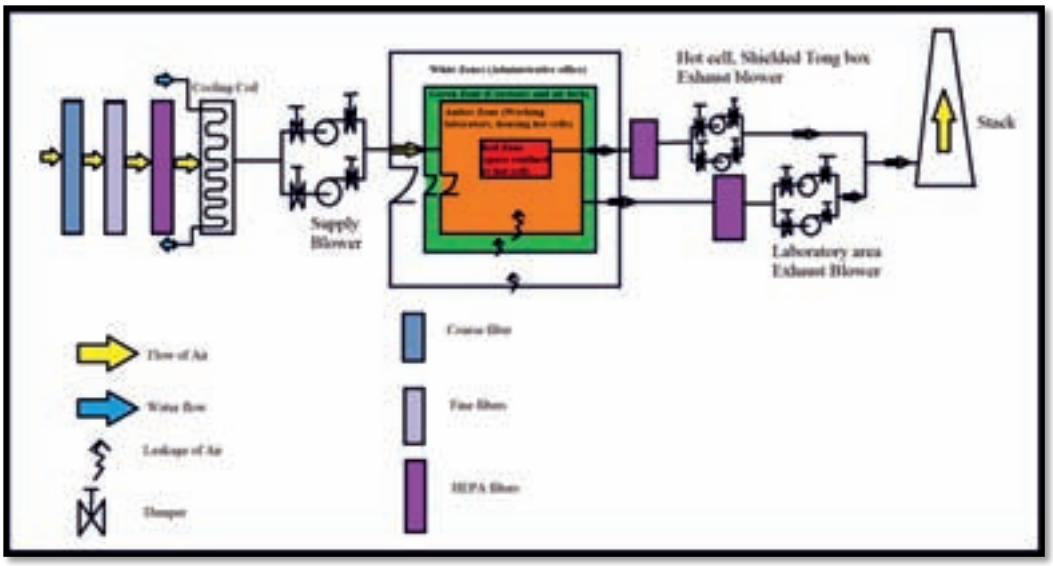

Fig: 1: A typical arrangement of AC and Ventilation system of a facility handling Radioactive material

of bundle of pipes and thin sheet and cold water flowing through bundle of pipes). As air flows over these cold tube bundles, air loses its energy and cools down. Energy lost by air is gained by cooled water flowing inside tube bundles and water gets heated up. Cooling of air and heating of water inside the tube is a continuous process. Humidity is also controlled using this cooling coil. For all this processes, engineering and precise calculation is required, and for these processes, we require air to be flowing, so as to make air flow, blower (also referred as fan) is required. Once filtration and cooling of air is complete, air is ready to be transferred to laboratory zone which is sent to the laboratories through network of ducts.

Ventilation is the circulation of air through network of ducts to whole facility.

In radioactive facility, ventilation system serves multiple purposes. It provides operator protection by maintaining the required depressions (differential pressure between different zones; Fig: 1). At the same time, ventilation needs to collect contaminated air flow, so as to control airborne activity, which could be released from the facility. It maintains directional flow, specified number of air changes inside radioactive facility [1], temperature inside working zone, humidity, derived air concentration under limit (DAC) etc. Also, A radioactive facility normally has no windows or natural ventilation cowls for providing additional air flow. It will often be necessary where hot periods can occur to provide cooling (AC) to the inlet air to maintain a comfortable working condition for working personnel.

General purposes of Ventilation system

1. For controlling the airborne contamination within safe working levels. This contamination can be result of normal operation, maintenance, and accident conditions.
2. For filtration and monitoring of the air supply on a “once through basis”.
3. For supplying fresh air on “once

through basis" after filtration. This filtration of supply air is done to keep the dust concentration to a minimum in working laboratory, in order to reduce the surface contamination and reduce the dust load on the exhaust filters.

4. For maintaining directional flow. This directional flow ensures the flow from the point of least contamination to the point of greatest contamination, which protects personnel working inside laboratory from spread of contamination by a haphazard ventilation air pattern.
5. For filtration of the exhaust air before releasing the air back to atmosphere.
6. For monitoring contaminants in the working laboratory and release to the environment.

Classification of Active Areas

Any radioactive facility is classified in four types of zones [1], according to the potential magnitude of the radioactive hazard present in that area. A common classification of zones are as follows:

1. **White zone:** Clean area, free from any radioactive contamination. This area is also unrestricted for entry of any personnel working inside this Laboratory. Examples are administrative office, library, canteen or any inactive service areas.
2. **Green zone:** This area is regularly cleaned and monitored, and hence, substantially clean. One can find radioactive contamination in this area only in exceptional scenario. Typical examples are, corridors and Health Physics rooms.
3. **Amber zone:** Some surface contamination must be expected in this area and air contamination will occasionally exceed the percentage allowable DAC. Examples are laboratory containing glove boxes, active maintenance areas and cell intervention areas etc. Occupancy in these areas must be restricted.
4. **Red zone:** Normally no access is envisaged for this area, because, contamination levels in these areas are expected to be high.

For effective design of ventilation system, air flow pattern in a radioactive facility should be from outside of the nuclear facility to inside of the nuclear facility, and, opposite of this should never happen. This directional flow arrangements ensure that any contamination inside laboratory is not leaked to immediate surroundings, keeping the operator in radioactive facility, safe. To make this flow of air from outside to inside, pressure inside the laboratory is maintained at lower pressure compared to its surroundings (flow of fluid always happens from high pressure area to low pressure area). Also, inside the laboratory, directional flow arrangement is made by keeping hot cells or shielded tong boxes to lower pressure compared to other laboratory areas of the room, to prevent any contamination from leaking outside the hot cell or shielded tong box confinements. So, it can be concluded that in any radioactive facility, containment handling radioactive material remains under lower pressure compared to laboratory room housing it, and again, room remains at lower pressure compared to surrounding area. To maintain pressure difference between white zone and green zone, between green zone and amber zone and between amber zone and red zone, exhaust of air is done at slightly greater rate compared to supply of air. General exhaust rate of air is 10% to 15% [1] higher compared

to supply rate and air balancing is done to achieve the required pressure difference between different zones. Air also leaks from high pressure area to low pressure area, which, is from white zone to green zone, from green zone to amber zone, from amber zone to red zone.

Fresh Air supply system

One unique characteristic of nuclear facility ventilation system is, that the ventilation here is essentially 'once through' type of system [1]. In industries, the concept of recirculation of cold air is followed. This recirculation of air means some fraction of cold air collected from the inside of the laboratory is resupplied to laboratory back, by mixing it with the fresh air taken from atmosphere, and rest of the fraction of cold air is released to atmosphere. Total air cannot be recirculated as personnel inside laboratory breathes out CO_2, and hence, it is imperative to keep this contaminant air under certain levels. Fresh air needs to be introduced in the laboratory. At the same time, 100% of fresh air supply to laboratory will lead to higher power consumption, and hence, a balance must be struck between 100% fresh air supply and 100% recirculation air supply to laboratory. But, inside the radioactive facility, personnel safety is paramount. So as to have efficient AC and Ventilation system inside the radioactive facility, this recirculation type of ventilation system isn't warranted, as it increases the chances of contamination. If any contamination is present in the laboratory, and the air is recirculated, it increases the risk of inhalation by any operator inside the laboratory. In radioactive facility, 'once through' ventilation system is employed, where total air requirement for working laboratory is taken from atmosphere and then this air is filtered through three sets of filters (coarse filter, fine filter, and HEPA filter). Air is then cooled through cooling coil and then supplied to working laboratory through network of ducts. This total amount of supplied air is collected through exhaust grilles and network of ducts using an exhaust blower and exhausted back to atmosphere through a stack and no portion of supplied air is recirculated. Also, a monitoring system is employed for exhaust air to determine that exhaust air is not contaminated from any radioactive material being handled in a production laboratory, and is discharged to atmosphere through stack only after ensuring the absence of any contamination.

Air Changes in Ventilated area

In working area, so as to maintain the safe working levels of airborne contamination, there should be sufficient changes of air. A wide range of air change rate have been used in radioactive facilities and is often expressed in terms of air changes per hour (ACPH). Generally, in most active area i.e., red zone, 20 ACPH [2], are not uncommon.

Air distribution in working area should be designed properly so that not even any single pocket of air remains stagnant. It is necessary to ensure that 'short circuiting' of air between inlet and outlet does not occur. Smoke tests can be performed to ensure that the air flow pattern is as per designed system.

Exhaust Air System

Since primary function of ventilation system is “protection of personnel”, the user is more concerned with the exhaust system than with the supply characteristic.

Exhaust system of a radioactive facility is, generally, designed to keep the exhaust air from radioactive laboratory area i.e. amber zone, and exhaust air from hot cells, shielded tong box or glove box i.e. red zone, separate. This is done because Glove boxes have different requirement in terms of availability, safety, pressure differential, amounts of air and the risk of contamination. Exhaust system is designed in such a manner that its capacity is not influenced by negative pressure inside laboratory and the cleanliness of the filter. The main features of an exhaust system serving radioactive laboratory are:

- Exhaust air is filtered through HEPA filter, and. wherever necessary. sorption filter is also employed.
- High availability with partial or total redundancy.
- Whole exhaust system from collection grilles to stack, should be leak tight.
- Zoning philosophy for air movement for prevention of the backflow of contaminated air.
- High differential pressure is maintained.
- Corrosion resistance and ease of decontamination.
- Control device for maintaining constant flow in exhaust side operation, even with different resistances.
- Monitoring of exhaust air for contamination.

Exhaust air collected from radioactive laboratory area is filtered through HEPA filters to prevent any radioactive contamination discharge to atmosphere, and then, exhausted to atmosphere through stack. Whereas, exhaust air collected from hot cells, shielded tong boxes or glove boxes is first filtered through HEPA filters or combination of HEPA filter and charcoal filters located just outside these confinements. The exhaust systems are then once again filtered through HEPA filters and only then exhausted to atmosphere through stack. This is done because volume of exhaust air from red zone is smaller but requires additional treatment (filtration) compared to amber zone exhaust air. These two separate streams of air are mixed only before these streams enters stack to be released to atmosphere. Exhaust air from white zone and green zone leaks to amber zone, and then together, the air is exhausted along with amber zone exhaust air.

Conclusion

AC and Ventilation system are essential parts of any radioactive facility, and plays vital role is creating a comfortable and safe working conditions inside working laboratory for operators. Also, it protects environment from discharge of any contaminants. Successful commissioning of a radioactive facility can only be considered when Air Conditioning and Ventilation system of that facility works according to the specified objectives. In designing the ventilation system for the laboratory, handling low and intermediate radioactive level radioactive waste, the following consideration should be considered:

a. Type of contamination zones that will be needed. White and green zone may be sufficient for handling radioactive tracers, but radioactive production laboratory requires all the four zones.

b. A ventilation system should provide directional flow, from white zone to red zone and increasing number of air changes per hour in each

successive zone from white to red zone.

c. Ventilation design should ensure the radionuclides in working areas remain under Derived Air Concentration (DAC), and discharge to atmosphere should also meet applicable regulations.

Changing and in-situ testing of HEPA filters is an important aspect of the ventilation system of radioactive laboratory, and due deliberations must be given. Fans, silencers, dampers, and ductworks are well developed technology. The main task of the designer is to select the best combination of these equipment to provide the desired result.

The choice of a method may depend on the standards and regulatory requirements.

Therefore, in the initial stage of conception of a nuclear facility only, it is essential for designer, regulatory authority and operational staff, to consider all the criteria in the light of the testing, philosophy, and methodology.

References

1. AERB Safety guide, AERB/RF-RS/SG-2.
2. IAEA Technical report series no. 292.

Compiled, Edited and Published by
Dr. Tarveen Karir
Sr. Manager, Scientific Information Resources & Publications,
Technical Services Division,
Board of Radiation & Isotope Technology, DAE

Printed by
M/S Sundaram Art Printing Press
Wadala, Mumbai